TECHNISCHE
UNIVERSITÄT
WIEN
Vienna University of Technology

INSTITUT FÜR
MECHANIK UND
MECHATRONIK
Mechanics & Mechatronics

DIPLOMARBEIT

Design, implementation, and experimental validation of a model predictive control scheme for a small-scale refrigerated truck

ausgeführt zum Zwecke der Erlangung des akademischen Grades eines Diplom-Ingenieurs
unter der Betreuung von

Dipl.-Ing. Markus Fallmann

und unter der Leitung von

Ao.Univ.Prof. Dipl.-Ing. Dr.techn. Martin Kozek
Institut für Mechanik und Mechatronik
Abteilung für Regelungstechnik und Prozessautomatisierung

eingereicht an der Technischen Universität Wien

Fakultät für Maschinenwesen und Betriebswissenschaften

von

Maximilian Lösch
[redacted]

Eidesstattliche Erklärung

Ich erkläre an Eides statt, dass ich die vorliegende Arbeit selbständig angefertigt, keine anderen als die angegebenen Hilfsmittel benutzt und alle aus ungedruckten Quellen, gedruckter Literatur oder aus dem Internet im Wortlaut oder im wesentlichen Inhalt übernommenen Formulierungen und Konzepte gemäß den Richtlinien wissenschaftlicher Arbeiten zitiert, durch Fußnoten gekennzeichnet bzw. mit genauer Quellenangabe kenntlich gemacht habe.

Wien, am 21. Oktober 2022

Maximilian Lösch

Kurzfassung

Kühlfahrzeuge sind für die Kühlketten von Lebensmitteln und pharmazeutischen Produkten von großer Bedeutung und die Nichteinhaltung der Temperaturanforderungen führt zu hohen finanziellen Verlusten. Aufgrund ihrer hohen Treibhausgasemissionen tragen Kühlfahrzeuge aber auch erheblich zur globalen Erwärmung bei. Emissionsbeschränkungen und wirtschaftliche Aspekte legen daher die Entwicklung energieeffizienterer Kühlfahrzeuge nahe, die auch Temperaturbeschränkungen sehr genau einhalten können. Hierfür ist nicht nur moderne Hardware wie hochwertige Kühlaggregate von großer Bedeutung, sondern auch durchdachte Steuerungsalgorithmen. Vor allem Türöffnungen haben einen großen Einfluss auf die Energieeffizienz und die Einhaltung der Referenztemperatur. Speziell kleine Kühlfahrzeuge, die oft für den Nahtransport eingesetzt werden, verzeichnen deutlich häufiger Türöffnungen als große Kühlfahrzeuge, die für den Langstreckentransport verwendet werden. Daher beschäftigt sich diese Arbeit mit einem modellprädiktiven Regelkonzept für kleine Kühlfahrzeuge, welches Türöffnungen explizit berücksichtigt. Um den Regler unter realen Bedingungen zu testen, wurden experimentelle Untersuchungen an einem Prüfstand angestellt. Das mathematische Modell der Reglelstrecke wurde daran identifiziert und validiert und zeigt eine sehr gute Übereinstimmung mit den Messdaten. Da die Dynamik sowohl durch schaltende als auch kontinuierliche Größen beschrieben wird, handelt es sich um ein hybrides Modell. Um die Leistungsfähigkeit des Reglers zu evaluieren wurde ein Vergleich mit einem Proportional-Integral Regler angestellt, der den derzeitigen Stand der Technik bei Temperaturreglern für Kühlfahrzeuge darstellt. Experimentelle Ergebnisse zeigen, dass die modellprädiktive Regelung im Vergleich zur Proportional-Integral-Regelung bis zu 34,2% der elektrischen Energie während einer Türöffnung einsparen kann, wenn die Türöffnung im Voraus bekannt ist. Insgesamt konnte der Regler während eines 5,25 stündigen Versuchs mit 4 Türöffnungen 17,4% an Energie im Vergleich zum Referenzregler einsparen. Darüber hinaus wurde der Regler in dieser Arbeit mit einem weiteren modellprädiktiven Ansatz verglichen. Die Arbeit zeigt, dass mit einem fortschrittlichen Regelungssystem für ein Kühlfahrzeug, das das Öffnen der Türen explizit berücksichtigt, im Vergleich zu einem herkömmlichen Regler große Mengen an Energie eingespart werden können.

Abstract

Energy consumption of refrigerated road transport will rise significantly in the future. In particular, frequent door openings, typical for small-scale refrigerated trucks, strain the energy efficiency and compliance with temperature requirements of such trucks. Numerous improvements have been made regarding the hardware in recent years, but little was done in terms of advanced temperature controllers to take advantage of modern hardware. Especially refrigeration systems with a secondary storage loop show the potential to benefit greatly from dedicated control schemes. This thesis proposes a sophisticated model-based predictive temperature controller for a small-scale refrigerated truck, which explicitly considers door openings in the control action. Therefore, a low-order model suitable for control application was developed. The switching behavior of the components was described with a discrete hybrid automaton modeling approach, resulting in a hybrid model. The proposed model and controller were evaluated using experimental measurements on a test bench. Applied to the experimental setup, the presented hybrid model has an excellent fit to the measurement data and consequently provides accurate predictions to the controller. To evaluate the performance of the proposed temperature controller, it is compared with a state-of-the-art proportional-integral controller. Experimental results show that the predictive controller can reduce energy consumption by up to 34.2% during a single door opening compared to the reference controller, with similar performance in terms of temperature compliance. In total, the model-based predictive controller saved 17.4% of energy during a 5.25 hour experiment with 4 door openings. Moreover, another model-based predictive controller is presented for reference. This thesis shows that a sophisticated predictive temperature controller can exploit the full potential of modern refrigeration hardware and achieve substantial energy savings.

Contents

Chapter 1

Introduction

In total the global cold chain market was valued at 210 billion USD in 2020 and it is expected to approximately triple its revenue until 2028 [1]. Cold chain systems are crucial for food distribution and pharmaceutical products. Especially the cold chain of the pharmaceutical industry has stringent requirements to maintain the efficacy and safety of pharmaceuticals. But perishable food also benefits greatly from cold chains due to reduced water, flavor, and nutrition loss and increased shelf-life [2]. Refrigerated road transport plays a critical role in cold chains. Significant amounts of food and pharmaceutical products are lost due to temperature excursions during transportation [3, 4]. Therefore, it is essential that the cargo temperature can be regulated accurately to adhere to temperature requirements regardless of disturbances such as door openings. Especially small-scale refrigerated trucks that conduct multi-drop delivery face substantial difficulties maintaining the temperature of the cargo since a single delivery run can sometimes include up to 50 door openings [5]. Furthermore, it is also essential that the refrigeration system operates with high energy efficiency since approximately 15% of the world's fossil fuel energy is used for refrigerated food transportation alone [6].
However, not much has been done in terms of temperature controllers that strive to both, fulfilling temperature restrictions and gain high energy efficiency. Some authors [7–9] proposed a model-based temperature controller but neglected door openings in their model, which makes the controller unsuitable for use in a small-scale refrigerated truck. Others [10] included door openings in their model-based controller but excluded the energy consumption from their control criterion.
Particularly elaborate refrigeration systems, such as those with a secondary cooling loop, require dedicated control schemes to realize their full potential [11, 12]. Fallmann et al. [13] dealt with modeling a small-scale refrigerated truck with a secondary loop refrigeration unit and included door openings as an actual connection between the air inside the cooling chamber and the ambient air. Their system is schematized in Fig. 1.1. Such a truck, which is frequently subject to door openings, can greatly benefit from dedicated control schemes which can exploit the advantages of cooling units with storage loops.
For the direct control of the cargo temperature, a model of the load is necessary, which

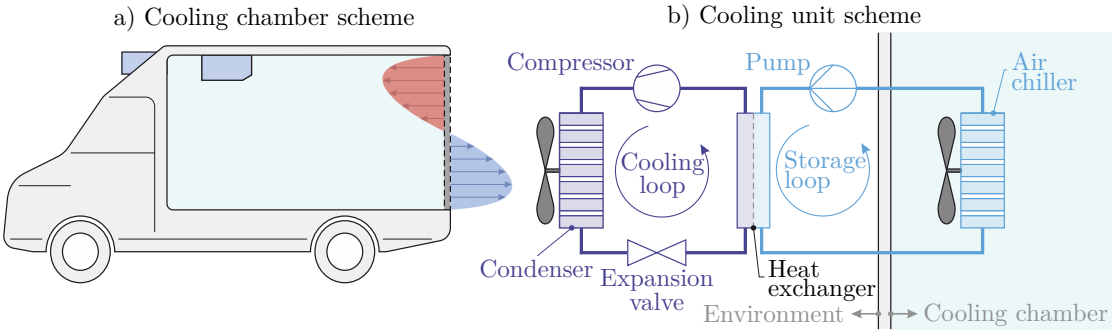

Figure 1.1: Schematic illustration of a small-scale refrigerated truck with a secondary loop refrigeration unit. The cooling unit comprises a conventional cooling loop and a storage loop which acts as a reservoir for thermal energy. Figure adapted from [13].

requires precise knowledge of the physical properties of the cargo. However, this approach is not practical for a small-scale refrigerated truck often loaded and unloaded with various cargo. Even if the cargo with all its parameters is known exactly, the initial temperature when loading new cargo must be estimated, which can also lead to considerable uncertainties. Therefore, in many control applications for refrigerated trucks, the temperature of the air is regulated rather than the cargo temperature [10]. This thesis proposes a sophisticated model-based temperature controller for the air inside the cooling chamber of a small-scale refrigerated truck with a secondary loop refrigeration unit. The controller explicitly considers the energy consumption and temperature excursions in determining control variables. For reference, another model-based controller, which is more limited in the selection of the control variables and has a reduced model, and a state-of-the-art proportional-integral (PI) controller are introduced. A specially designed test bed was used to examine the controllers in real world conditions, since it is costly to perform tests with an actual refrigerated vehicle.
The remainder of this thesis is organized as follows: First, in Chapter 2, a model of the test bed for small-scale refrigerated truck with a secondary loop refrigeration system is derived. Then the different temperature control schemes are proposed in Chapter 3. In Chapter 4, the model and the controller are evaluated on the experimental setup, and the results are discussed in Chapter 5. Finally, a summary of the work and its limitations is given in Chapter 6.

Chapter 2

Modeling

This chapter describes the modeling of the cooling chamber and the cooling unit. First, in Section 2.1, the system to be modeled is described in every detail. Subsequently, an overview of the different modeling approaches of cooling chambers and cooling modules in the literature is given (Section 2.2). Finally, in Section 2.3, a mathematical model of the system is derived.

2.1 System description

The test bed of the small-scale refrigerated truck with a secondary loop refrigeration unit comprises the cooling chamber with insulated walls, a door, and two cooling units that generate the cooling capacity, see Fig. 2.1. In the further proceedings of this thesis, the two identical cooling units are always operated in parallel. Therefore, to simplify the notation, the cooling units in the system will be combined into a single cooling unit with twice the cooling capacity, and from now on, only this combined cooling unit will be referred to.
The cooling unit consists of a thermoelectric cooler (TEC) in the center with a heat sink on each side of the module. By applying an electric current $I_{\text{tec}} \in \mathbb{R}_{\geq 0}$ the TEC can create a heat flow $\dot{Q}_{\text{tec}} \in \mathbb{R}$ that cools one side (cold side) and heats the other (hot side). The status (off/on) of the TEC is described by $s_{\text{cu}} \in \{0, 1\}$, resulting in $I_{\text{tec}} = 0$ when the TEC is turned off. A water-cooling block installed on the hot side of the TEC is fed with water at temperature $T_{\text{wtr}} \in \mathbb{R}$. On the cold side of the TEC, an air-cooled heat sink with temperature $T_{\text{hs}} \in \mathbb{R}$ is used to store and transfer thermal energy to the air inside the cooling chamber. A fan mounted to the air-cooled heat sink can evoke a heat flow $\dot{Q}_{\text{cu}} \in \mathbb{R}$ by either natural or forced convection by switching the fan on or off $s_{\text{f}} \in \{0, 1\}$. The air-cooled heat sink is an analogy to the secondary storage loop of the refrigerated truck's cooling unit, as it can also store thermal energy. However, the thermal storage of the heat sink with the TEC has significantly higher losses than the storage loop of a refrigerated truck due to the large heat losses from thermal conduction through the TEC. A subordinate controller is implemented to compensate for the heat losses through the TEC when the cooling unit is turned off to achieve the same system

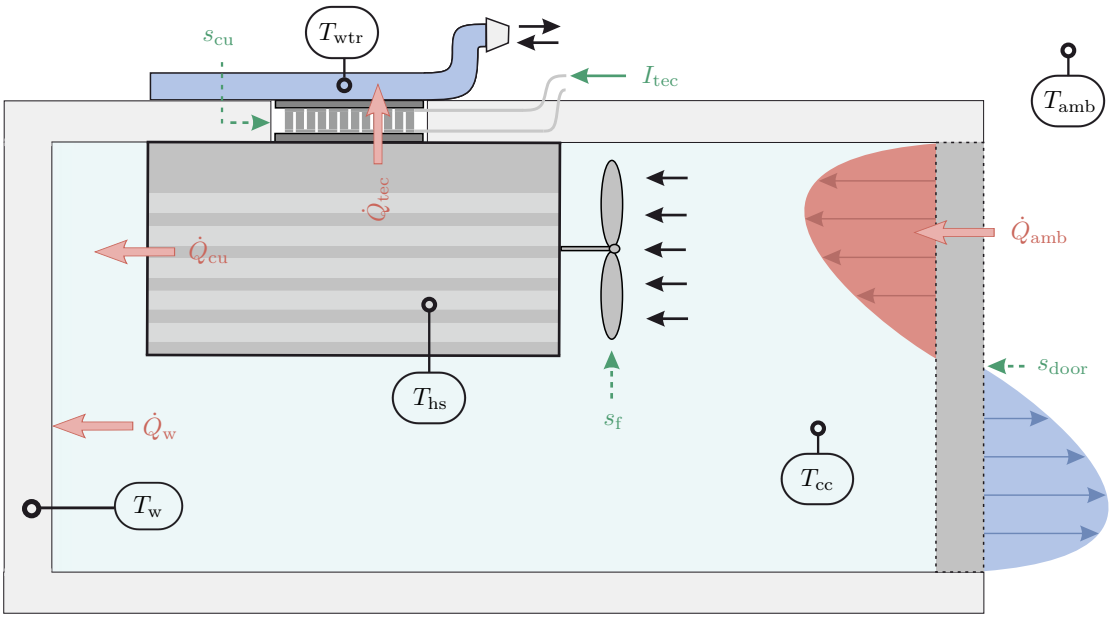

Figure 2.1: Illustration of the cooling chamber and the cooling unit with important modeling variables. The temperature of the air inside the cooling chamber T_{cc}, the ambient air T_{amb}, the wall T_w, the heat sink T_{hs}, and the water for the water-cooling T_{wtr} are highlighted due to their importance for modeling. The heat flows between the air inside the cooling chamber and the wall $\dot{Q}_w$, the heat sink and the air inside the cooling chambers $\dot{Q}_{cu}$, the heat sink and the water cooling $\dot{Q}_{tec}$, and the ambient air with the air inside the cooling chamber $\dot{Q}_{amb}$ are indicated by red arrows. The heat transfer in the event of a door opening s_{door} is especially highlighted. The fan mounted to the heat sink can increase the airflow through the heat sink when it is active, indicated by its status s_f. The thermoelectric cooler is operated with a current I_{tec} and its status is defined by the variable s_{cu}.

dynamics [14].
The insulated walls act as a thermal mass with the temperature $T_w \in \mathbb{R}$ and can exchange a heat flow $\dot{Q}_w \in \mathbb{R}$ with the air inside the cooling chamber. The heat flow from the environment to the inside of the cooling chamber is described by $\dot{Q}_{amb} \in \mathbb{R}$. This heat flow depends strongly on the status of the door $s_{door} \in \{0, 1\}$. The air inside the cooling chamber has the temperature $T_{cc} \in \mathbb{R}$.

2.2 Modeling approaches in the literature

There are many different models of varying complexity in the literature for modeling TECs. The most sophisticated models describe the TEC three-dimensional with temperature-dependent material parameters [15, 16]. Those models achieve the high-

est accuracy but require a lot of computational effort [17]. Reduced models assume a thermal equilibrium and constant material parameters, which lead to an algebraic equation for the heat flow on each side of the TEC [18–20]. In a steady state, the equilibrium model with constant material parameters gives nearly the same results as the three-dimensional model with temperature-dependent material properties. However, the equilibrium model is significantly faster [21].
Various approaches exist for modeling the temperature of the air inside a cooling chamber. Modeling the interior of the cooling chamber with distributed parameters using the method of computational fluid dynamics leads to models with high resolution. These models can describe the volume, mass, and energy flow during a door opening very well, as shown by Ben Taher et al. [22]. Due to the high computational cost of computational fluid dynamic models, reduced models with concentrated parameters are often used for modeling the air temperature of a cooling chamber in control applications [8, 9].
To model the heat flow during a door opening Lafaye De Micheaux et al. [23] derived a system of ordinary differential equations from first principles. Luchini et al. [10] used a predefined heat flow profile to model the door opening for their control application.
In the literature, the insulated walls of the cooling chamber are usually modeled by thermal capacities connected in series. This reproduces the slow dynamics of the heat flow from the environment to the inside of the cooling chamber, but also the fast dynamics directly affecting the air temperature inside the cooling chamber [10, 13, 23].
The heat flow due to the absorption of solar radiation is included in some models in the literature. However, the influence of thermal radiation on the inside of the cooling chamber has comparably slow dynamics and is negligible if the vehicle moves, due to the increased convective heat flow between the outer wall and the environment [24].

2.3 Model description

The derived model is based on above discussed modeling approaches in the literature, the model of a small-scale refrigerated truck with a secondary loop cooling system proposed by Fallmann et al. [13], and on open-loop experiments conducted on the experimental setup. Care was taken to account for both, the slow dynamics of the system when the door of the cooling chamber is closed and the fast dynamics when the door is open. Moreover, with model-based control schemes, not only an accurate model is of great importance, but also a low model order to reduce computational costs.
The model equations are presented in Section 2.3.1. Unknown model parameters were estimated based on the conducted open-loop experiments described in Section 2.3.2. Subsequently, the derived model was linearized and discretized for use in model-based control schemes, see Section 2.3.3.

2.3.1 Model equations

The system described above is a hybrid system, comprehending both continuous and binary variables. This kind of system lends itself to a formulation using discrete hybrid automatons (DHAs), as described by [25]. With this approach, the binary and continuous variables can be separated, which facilitates the description of the model and the formulation of a control algorithm. Here, the binary variables appear only in the inputs and disturbances, reducing the DHA to a switched affine system (SAS) and a mode selector (MS). The task of the MS is to select the corresponding model of the SAS based on the binary variables. All the SAS models use the same state, input, and disturbance vector, so the transition from one mode to the other is done simply by passing the recently calculated state vector to the next model. To formulate the MS the $n_{\mathrm{ub}} = 2$ binary control variables are summarized in the vector of controllable inputs $\boldsymbol{u}_{\mathrm{b}} \in \mathbb{R}^{n_{\mathrm{ub}}}$ according to

$$\boldsymbol{u}_{\mathrm{b}}(t) \coloneqq \begin{bmatrix} s_{\mathrm{cu}}(t) \\ s_{\mathrm{f}}(t) \end{bmatrix}, \tag{2.1}$$

written in continuous time $t \in \mathbb{R}_{\geq 0}$. The status of the door is the only binary disturbance $v_{\mathrm{b}} \in \mathbb{R}$ in the model:

$$v_{\mathrm{b}}(t) \coloneqq s_{\mathrm{door}}(t) \tag{2.2}$$

Therefore, the MS must map the three binary variables to the resulting eight modes, as shown in Table 2.1.

Table 2.1: Classification of model modes depending on the status of the cooling unit s_{cu}, the status of the fan s_{f}, and on door openings s_{door}.

Mode $m(t)$	$s_{\mathrm{cu}}(t)$	$s_{\mathrm{f}}(t)$	$s_{\mathrm{door}}(t)$
1	0	0	0
2	1	0	0
3	0	1	0
4	1	1	0
5	0	0	1
6	1	0	1
7	0	1	1
8	1	1	1

To determine the active mode $m(t) \in \mathcal{M} = \{1, 2, \ldots, 8\}$ the function of the MS, $f_{\mathrm{MS}} : \{0,1\}^3 \to \mathcal{M}$, is defined according to

$$m = m(t) = f_{\mathrm{MS}}\left(s_{\mathrm{cu}}(t), s_{\mathrm{f}}(t), s_{\mathrm{door}}(t)\right). \tag{2.3}$$

For brevity, the time dependency of the active mode is omitted from now on, and instead the mode dependency is explicitly stated where appropriate.
Each mode has an associated model belonging to the SAS. The SAS describes the dynamics of the system by transforming the state vector $\boldsymbol{x}_\mathrm{c} \in \mathbb{R}^{n_\mathrm{x}}$ with $n_x = 3$ continuous states given by

$$\boldsymbol{x}(t;m) \coloneqq \left[\; T_\mathrm{hs}(t;m), T_\mathrm{cc}(t;m), T_\mathrm{w}(t;m) \;\right]^\mathrm{T} \tag{2.4}$$

with the continuous input $u_\mathrm{c} \in \mathbb{R}$ according to

$$u_\mathrm{c}(t) \coloneqq I_\mathrm{tec}(t), \tag{2.5}$$

and the continuous disturbance vector $\boldsymbol{v}_\mathrm{c} \in \mathbb{R}^{n_\mathrm{vc}}$ with $n_\mathrm{vc} = 2$ measurable disturbances defined as

$$\boldsymbol{v}_\mathrm{c}(t) \coloneqq \left[\; T_\mathrm{wtr}(t), T_\mathrm{amb}(t) \;\right]^\mathrm{T}, \tag{2.6}$$

into the vector of the model outputs $\boldsymbol{y} \in \mathbb{R}^4$, defined as

$$\boldsymbol{y}(t;m) \coloneqq \left[\; T_\mathrm{hs}(t;m), T_\mathrm{cc}(t;m), P_\mathrm{tec}(t;m), P_\mathrm{f}(m) \;\right]^\mathrm{T}. \tag{2.7}$$

Cooling unit

As described above, the cooling unit consists of a TEC and two heat sinks; one water-cooled and one air-cooled. The water-cooled heat sink is fed with water at a constant temperature and it is assumed that the TECs hot side can be held at the same temperature as the water temperature. Furthermore, the temperature of the air-cooled heat sink on the cold side of the TEC has significantly slower dynamics than the temperature distribution in the comparatively thin TEC. Therefore, the equilibrium model described by [18–20] is used to model the TEC. The heat flow from the cold side of the TEC to the hot side is given by

$$\dot{Q}_\mathrm{tec}(t;m) = \alpha_1\, I_\mathrm{tec}(t)\, T_\mathrm{hs}(t;m) - \alpha_2\, I_\mathrm{tec}(t)^2 - \alpha_3 \left[T_\mathrm{wtr}(t) - T_\mathrm{hs}(t;m)\right] s_\mathrm{cu}(t) \tag{2.8}$$

with the unknown material parameters of the TEC $\alpha_i \in \mathbb{R}_{\geq 0}, i \in \{1,2,3\}$. In TEC literature, α_1 is usually referred to as the Seebeck coefficient, α_2 and α_3 as half the electrical resistance and the thermal conductance of the TEC, respectively. Note that the conductive heat flow through the TEC is zero when the cooling unit is off, which is evoked by a subordinate controller as mentioned above, and elaborated in detail in [14]. The power consumption of the TEC, $P_\mathrm{tec} \in \mathbb{R}$, can be calculated by

$$P_\mathrm{tec}(t;m) = \alpha_1 \left[T_\mathrm{wtr}(t) - T_\mathrm{hs}(t;m)\right] I_\mathrm{tec}(t) + 2\,\alpha_2\, I_\mathrm{cu}(t)^2. \tag{2.9}$$

The dynamics of the heat sink temperature are modeled by the heat balance equation yielding

$$\beta \frac{d}{dt} T_\mathrm{hs}(t;m) = -\dot{Q}_\mathrm{tec}(t;m) - \dot{Q}_\mathrm{cu}(t;m) \tag{2.10}$$

with the unknown heat capacity of the air-cooled heat sink $\beta \in \mathbb{R}_{\geq 0}$.

Cooling chamber

The heat transfer between the air inside the cooling chamber and the air-cooled heatsink can be written as

$$\begin{aligned}\dot{Q}_{\mathrm{cu}}(t;m) =&\gamma_1 \left[T_{\mathrm{hs}}(t;m) - T_{\mathrm{cc}}(t;m)\right] s_{\mathrm{f}}(t) + \dots \\ &\gamma_2 \left[T_{\mathrm{hs}}(t;m) - T_{\mathrm{cc}}(t;m)\right] \left[1 - s_{\mathrm{f}}(t)\right],\end{aligned} \tag{2.11}$$

where the type of heat transfer - forced or natural convection - is determined by the status of the fan with the respective unknown heat transfer coefficients $\gamma_1 \in \mathbb{R}_{\geq 0}$ and $\gamma_2 \in \mathbb{R}_{\geq 0}$. Since the fan can either be on or off, the power consumption of the fan $P_{\mathrm{f}} \in \mathbb{R}$ is modeled as

$$P_{\mathrm{f}}(m) = \zeta\, s_{\mathrm{f}}(t), \tag{2.12}$$

where $\zeta \in \mathbb{R}_{\geq 0}$ is the unknown parameter of the power demand of the fan. Another essential dynamic of the system is the wall temperature, which is described by

$$\kappa_1 \frac{d}{dt} T_{\mathrm{w}}(t;m) = \kappa_2 \left[T_{\mathrm{cc}}(t;m) - T_{\mathrm{w}}(t;m)\right] = \dot{Q}_{\mathrm{w}}(t;m) \tag{2.13}$$

with the unknown heat capacity and heat transfer coefficient of the wall $\kappa_i \in \mathbb{R}_{\geq 0}, i \in \{1,2\}$. In this formulation, the wall temperature is affected only by the air inside the cooling chamber and not by the ambient conditions, since these have much slower dynamics. The wall temperature is modeled first order to reduce the computational burden.

The heat transfer between the air inside the cooling chamber and the ambient air is composed of a term for the steady heat transfer through the wall and a term for the fast heat transfer due to an open door according to

$$\begin{aligned}\dot{Q}_{\mathrm{amb}}(t;m) =&\xi_1 \left[T_{\mathrm{amb}}(t) - T_{\mathrm{cc}}(t;m)\right] + \dots \\ &\xi_2 \left[T_{\mathrm{amb}}(t) - T_{\mathrm{cc}}(t;m)\right] s_{\mathrm{door}}(t),\end{aligned} \tag{2.14}$$

where $\xi_i \in \mathbb{R}_{\geq 0}, i \in \{1,2\}$ are the unknown heat transfer coefficients. The influence of other environmental factors, such as thermal radiation, was neglected here because they are either difficult to measure or have a negligible impact on the cooling chamber temperature.

The dynamics of the temperature of the air inside the cooling chamber are influenced by the above defined heat flows $\dot{Q}_{\mathrm{amb}}$, $\dot{Q}_{\mathrm{cu}}$ and, $\dot{Q}_{\mathrm{w}}$. Additionally, the power consumption of the fan act as a heat source that directly affects T_{cc}, yielding

$$\chi \frac{d}{dt} T_{\mathrm{cc}}(t;m) = \dot{Q}_{\mathrm{cu}}(t;m) + P_{\mathrm{f}}(m) - \dot{Q}_{\mathrm{w}}(t;m) + \dot{Q}_{\mathrm{amb}}(t;m) \tag{2.15}$$

with the unknown heat capacity of the air $\chi \in \mathbb{R}_{\geq 0}$.

2.3.2 Parameter identification

The model proposed above has $n_\theta = 12$ unknown model parameters, that can be summarized in the parameter vector $\boldsymbol{\theta} \in \mathbb{R}^{n_\theta}_{\geq 0}$ according to

$$\boldsymbol{\theta} = \Big[\alpha_1, \alpha_2, \alpha_3, \beta, \gamma_1, \gamma_2, \zeta, \kappa_1, \kappa_2, \xi_1, \xi_2, \chi\Big]^{\mathrm{T}}. \tag{2.16}$$

To obtain a numerically well-posed estimation, the parameter vector is linearly transformed so that all parameters have an similar order of magnitude, yielding the normalized parameter vector $\boldsymbol{\theta}'$ defined by

$$\boldsymbol{\theta}' \coloneqq \boldsymbol{C}_\theta^{-1}\, \boldsymbol{\theta} \tag{2.17}$$

with all normalized parameter values between 0.1 and 1. The transformation matrix $\boldsymbol{C}_\theta \in \mathbb{R}^{n_\theta \times n_\theta}$ contains the normalization coefficients of each parameter $c_\eta \in \mathbb{R}$ with $\eta \in \boldsymbol{\theta}$ in its diagonal according to

$$\boldsymbol{C}_\theta = \mathrm{diag}\Big[c_{\alpha_1}, c_{\alpha_2}, \dots\ c_\chi\Big]. \tag{2.18}$$

Then, the dynamics of the system can be described as

$$\dot{\boldsymbol{x}}(t;m) = \boldsymbol{f}_{\mathrm{x}}\Big(\boldsymbol{x}(t;m), u_{\mathrm{c}}(t), \boldsymbol{v}_{\mathrm{c}}(t); \boldsymbol{\theta}'\Big) \tag{2.19a}$$

$$\boldsymbol{y}(t;m) = \boldsymbol{f}_{\mathrm{y}}\Big(\boldsymbol{x}(t;m), u_{\mathrm{c}}(t), \boldsymbol{v}_{\mathrm{c}}(t); \boldsymbol{\theta}'\Big) \tag{2.19b}$$

with the state function $\boldsymbol{f}_{\mathrm{x}} : \mathbb{R}^{6+n_\theta} \to \mathbb{R}^{n_x}$ and the output function $\boldsymbol{f}_{\mathrm{y}} : \mathbb{R}^{6+n_\theta} \to \mathbb{R}^4$. For the estimation of the parameter vector, $n_{\mathcal{I}}$ experiment data sets $\mathcal{I}_j, j \in \{1, \dots, n_{\mathcal{I}}\}$ with $n_k(\mathcal{I}_j)$ samples each are used. With that data, the estimated normalized parameter vector $\boldsymbol{\theta}'^*$ can be calculated by

$$\boldsymbol{\theta}'^* = \arg\min_{\boldsymbol{\theta}'} J_{\mathrm{Id}}\Big(\boldsymbol{\theta}'\Big) \tag{2.20}$$

with the objective function $J_{\mathrm{Id}} \in \mathbb{R}_{\geq 0}$ defined as

$$J_{\mathrm{Id}}\Big(\boldsymbol{\theta}'\Big) = \sum_{j=1}^{n_{\mathcal{I}}} \sum_{k=1}^{n_k(\mathcal{I}_j)} \Big[\boldsymbol{y}(k;m) - \boldsymbol{y}^{\mathrm{meas}}(k)\Big]^{\mathrm{T}} \Big[\boldsymbol{y}(k;m) - \boldsymbol{y}^{\mathrm{meas}}(k)\Big]. \tag{2.21}$$

Thereby, the quadratic deviation between the simulated model output $\boldsymbol{y}$ and the measured output vector $\boldsymbol{y}^{\mathrm{meas}} \in \mathbb{R}^4$ is penalized at every sampling instance $k \in \mathbb{R}_{\geq 0}$.

2.3.3 Linearization and discretization

The model is linearized to be able to use the special formulation of DHAs. Note that the nonlinear model is used to determine the unknown model parameters as described above, and only then is the system linearized.
The only nonlinear terms in the derived model can be found in the first and second

term of the heat flow equation of the TEC, see (2.8). The subordinate nonlinear heat flow of the TEC, $\dot{Q}_{sub}^{\text{nonlin}} \in \mathbb{R}$, is therefore defined as

$$\dot{Q}_{sub}^{\text{nonlin}}(I_{\text{tec}}, T_{\text{hs}}) = \alpha_1 \, I_{\text{tec}} \, T_{\text{hs}} - \alpha_2 \, I_{\text{tec}}^2. \tag{2.22}$$

For easier readability, the time and mode dependencies of the subordinate heat flow are omitted. The nonlinear model was linearized in two different manners, shown in Fig. 2.2. With the first method, the linearized heat flow $\dot{Q}_{sub}^{\text{lin},1} \in \mathbb{R}$ depends on both I_{tec} and T_{hs} according to

$$\dot{Q}_{sub}^{\text{lin},1}(I_{\text{tec}}, T_{\text{hs}}) = \lambda_1 \, T_{\text{hs}} + \lambda_2 \, I_{\text{tec}} + \lambda_3 \tag{2.23}$$

with the fitting parameters $\lambda_1 \in \mathbb{R}$, $\lambda_2 \in \mathbb{R}$, and $\lambda_3 \in \mathbb{R}$. The unknown parameters were fitted by least squares to the nonlinear heat flow to achieve the best fit in the current interval between $I_{\text{tec}}^{\text{lin,min}} \in \mathbb{R}_{\geq 0}$ and $I_{\text{tec}}^{\text{lin,max}} \in \mathbb{R}_{\geq 0}$ and the heat sink temperature interval between $T_{\text{hs}}^{\text{lin,min}} \in \mathbb{R}_{\geq 0}$ and $T_{\text{hs}}^{\text{lin,max}} \in \mathbb{R}_{\geq 0}$.
The second linearized heat flow $\dot{Q}_{sub}^{\text{lin},2} \in \mathbb{R}$ is directly proportional to I_{tec} and not depending on the heat sink temperature, yielding

$$\dot{Q}_{sub}^{\text{lin},2}(I_{\text{tec}}) = \lambda_4 \, I_{\text{tec}}, \tag{2.24}$$

with a single fitting parameter $\lambda_4 \in \mathbb{R}$. This parameter is also determined using least squares to fit to the intervals $\left[I_{\text{tec}}^{\text{lin,min}}, \, I_{\text{tec}}^{\text{lin,max}}\right]$ and $\left[T_{\text{hs}}^{\text{lin,min}}, T_{\text{hs}}^{\text{lin,max}}\right]$. The motivation behind the two different linearization methods is that the first method approximates the nonlinear heat flow very accurately over a limited current and temperature range. In contrast, the second method is valid over a broader range. It must be noted that the linearized heat flow with method one is generally not zero when the current is zero. Thus, this linearization method performs very poorly for small currents. With the second linearization method, it is always ensured that the heat flow vanishes when the current is zero. However, the dependency on the heat sink temperature was neglected, making this linearization generally less accurate.
The linearized model that the model-based control applications will use has a reduced output vector that comprises only the temperature of the heat sink and the air temperature inside the cooling chamber. The two linearized models can be written in a state-space representation according to

$$\dot{\boldsymbol{x}}(t; m, l) = \boldsymbol{A}(m, l) \, \boldsymbol{x}(t; m, l) + \boldsymbol{B}(m, l) \, u_{\text{c}}(t) + \boldsymbol{E}(m, l) \, \boldsymbol{v}_{\text{c}}(t) + \boldsymbol{g}(m, l) \tag{2.25a}$$

$$\begin{bmatrix} T_{\text{hs}}(t; m, l) \\ T_{\text{cc}}(t; m, l) \end{bmatrix} = \boldsymbol{C}(m, l) \, \boldsymbol{x}(t; m, l) + \boldsymbol{D}(m, l) \, u_{\text{c}}(t) + \boldsymbol{F}(m, l) \, \boldsymbol{v}_{\text{c}}(t) + \boldsymbol{h}(m, l), \tag{2.25b}$$

with the system matrix $\boldsymbol{A} \in \mathbb{R}^{n_x \times n_x}$, input vector $\boldsymbol{B} \in \mathbb{R}^{n_x}$, system disturbance matrix $\boldsymbol{E} \in \mathbb{R}^{n_x \times n_{vc}}$, affine system vector $\boldsymbol{g} \in \mathbb{R}^{n_x}$, output matrix $\boldsymbol{C} \in \mathbb{R}^{2 \times n_x}$, feedthrough vector $\boldsymbol{D} \in \mathbb{R}^2$, output disturbance matrix $\boldsymbol{F} \in \mathbb{R}^{2 \times n_{vc}}$, and affine output vector $\boldsymbol{h} \in \mathbb{R}^2$. The dependency of the linearization method is denoted by parameter $l \in \{1, 2\}$.
Furthermore, the continuous state space system is discretized using zero-order hold with sampling time $T_{\text{s}} \in \mathbb{R}_{\geq 0}$ to subsequently use the model in a digital controller. The subscript d denotes the discretized matrices.

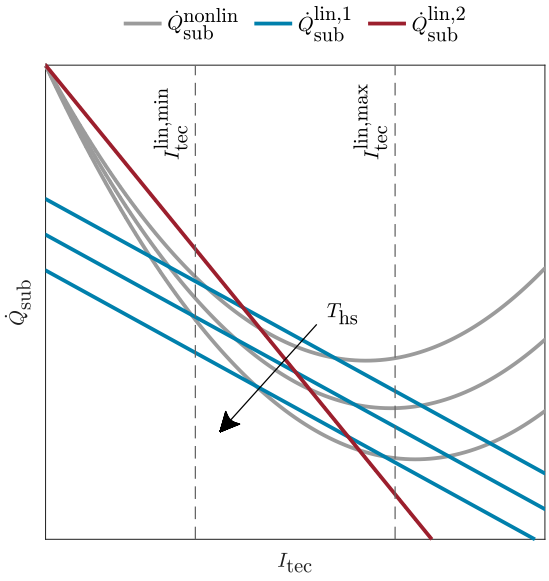

Figure 2.2: Visualization of the two different linearization methods for the subordinate heat flow of the TEC. The heat flows are plotted over the current of the TEC I_{tec} and at three different heat sink temperatures T_{hs}. The current interval for the fitting of the linearized heatflow is outlined with its lower and upper bound, $I_{\text{tec}}^{\text{lin,min}}$ and $I_{\text{tec}}^{\text{lin,max}}$ respectively.

Chapter 3

Controller design

This chapter proposes a temperature control concept for a small-scale refrigerated truck based on the model derived above. The conceptual architecture used for controlling the temperature inside the cooling chamber is depicted in Fig. 3.1. For ease of reading, the mode dependency is omitted from the notation in the following.
The plant (cooling chamber and cooling unit), the actuators, and the sensors form the extended plant, further described in Section 3.1. In Section 3.2, three different temperature controllers are described. For the model-based controllers, an accurate estimate of the current state of the plant is critical to the performance of the controller. Therefore, an observer is designed in Section 3.3.

3.1 Extended plant

The extended plant comprises the cooling chamber, the cooling unit, and all actuators and sensors. The plant is influenced by controllable inputs $\boldsymbol{u} = [u_\mathrm{c}\ \boldsymbol{u}_\mathrm{b}]$, measurable disturbances $\boldsymbol{v} = [\boldsymbol{v}_\mathrm{c}\ v_\mathrm{b}]$, and unknown disturbances $\boldsymbol{d}$.
The actuators convert the digital target values given by the temperature controller $\boldsymbol{u}^\mathrm{ref}$ into physical signals. The current flowing through the TEC is controlled by a buck converter, which steps down the constant input voltage from a voltage source to gain a mandated current. The buck converter is specially designed to meet the requirements of the TEC [26, 27]. A relay switches the fan and the TEC on or off.
For the temperature control of the plant, measurements of the system are fundamental. Therefore, various digital sensors are installed throughout the system to measure current, temperature, and power values at regular time intervals $T_\mathrm{s,meas} \in R_{\geq 0}$. It should be noted that the sampling time of the measurements is generally different from the sampling time of the temperature controller T_s.

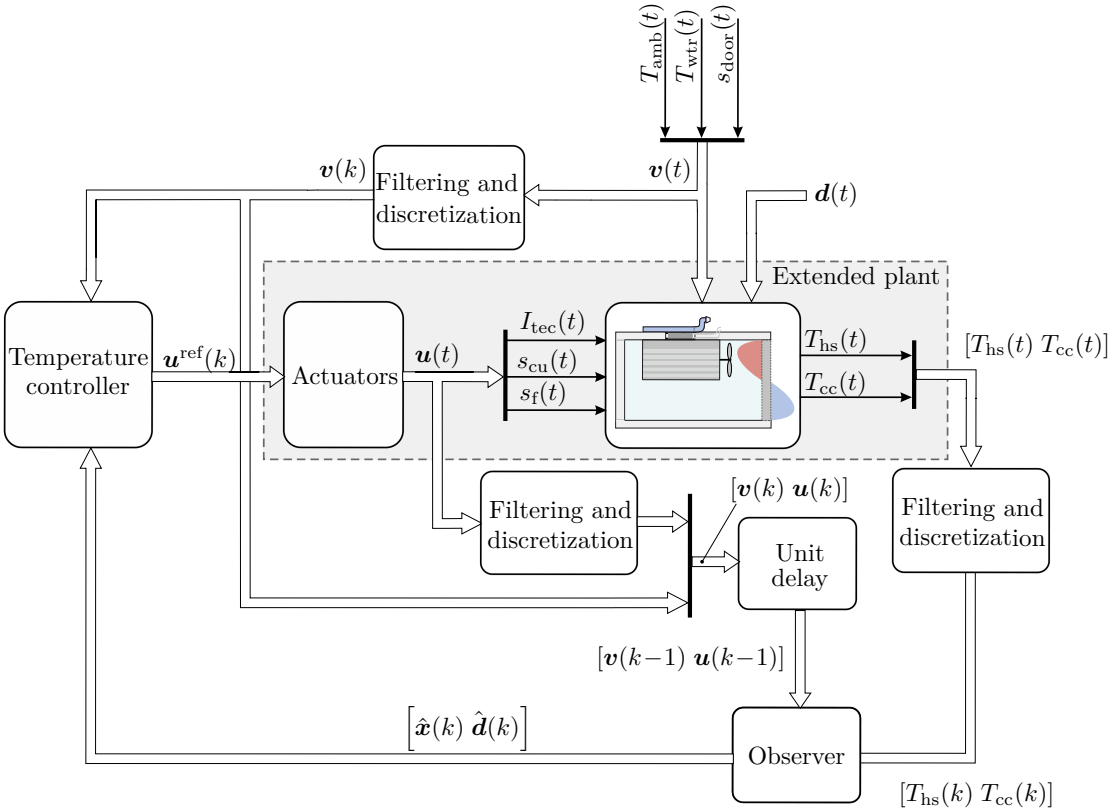

Figure 3.1: Conceptual architecture of the temperature controller for the cooling chamber. The extended plant consists of the plant itself and various actuators and sensors. The measurements of the plant are used by the observer to estimate the current state of the plant, which is then adopted by the controller to determine control variables.

3.2 Temperature controller

The purpose of the temperature controller is to regulate the temperature inside the cooling chamber. As in real-world applications, the desired temperature is usually not an exact temperature value but a temperature range [28]. The temperature controller should also aim to minimize energy consumption while maintaining a certain temperature window.
In many cases, the cooling units installed in small-scale refrigerated trucks are oversized for steady state operation and have a much higher cooling capacity than needed for holding the temperature at the desired value [24]. Manufacturers choose this design to allow fast and efficient cooling to the desired temperature from ambient conditions. In addition, the compressor is physically limited to a minimum and maximum speed at which it can operate. Therefore, it is usually not possible to maintain the desired temperature with a constant compressor speed, so the compressor must be turned on and off to maintain the temperature inside the cooling chamber. Constraints on the minimum and maximum current are introduced to obtain a similar behavior with the cooling units used in the test bed. In actual refrigeration units, the compressor and pumps cannot be turned on and off at will but must meet particular start-up and shut-down times. These restrictions are also transferred to the test bed, by imposing minimum up- and down-times on the fan and the cooling unit.
A total of three different temperature controllers is proposed, two model-based controllers with knowledge of future disturbances and a rule-based PI controller. In Section 3.2.1, a hybrid model predictive controller (HMPC) is described, which utilizes the maximum flexibility of the system. A derivative of the HMPC with limited flexibility in the choice of manipulated variables and reduced complexity of the model is presented in Section 3.2.2. In Section 3.2.3, a rule-based PI controller, which is state-of-the-art for temperature control, is defined.

3.2.1 Hybrid model predictive controller

The HMPC relies on a hybrid model for its predictions over a finite horizon with the length $N_\mathrm{p} \in \mathbb{N}$. The computation of the control inputs is based on an optimization problem, schematized in Fig. 3.2. The optimization variables are the predicted states, inputs and disturbances vectors over the prediction horizon. By stacking the respective

vectors, one gets

$$\boldsymbol{X}(k) \coloneqq \begin{bmatrix} \boldsymbol{x}(k|k) \\ \boldsymbol{x}(k{+}1|k) \\ \vdots \\ \boldsymbol{x}(k{+}N_\mathrm{p}|k) \end{bmatrix}, \boldsymbol{U}_\mathrm{b}(k) \coloneqq \begin{bmatrix} \boldsymbol{u}_\mathrm{b}(k) \\ \boldsymbol{u}_\mathrm{b}(k{+}1) \\ \vdots \\ \boldsymbol{u}_\mathrm{b}(k{+}N_\mathrm{p}{-}1) \end{bmatrix}, \boldsymbol{U}_\mathrm{c}(k) \coloneqq \begin{bmatrix} u_\mathrm{c}(k) \\ u_\mathrm{c}(k{+}1) \\ \vdots \\ u_\mathrm{c}(k{+}N_\mathrm{p}{-}1) \end{bmatrix}$$
$$\boldsymbol{V}_\mathrm{b}(k) \coloneqq \begin{bmatrix} v_\mathrm{b}(k) \\ v_\mathrm{b}(k{+}1) \\ \vdots \\ v_\mathrm{b}(k{+}N_\mathrm{p}{-}1) \end{bmatrix}, \boldsymbol{V}_\mathrm{c}(k) \coloneqq \begin{bmatrix} \boldsymbol{v}_\mathrm{c}(k) \\ \boldsymbol{v}_\mathrm{c}(k{+}1) \\ \vdots \\ \boldsymbol{v}_\mathrm{c}(k{+}N_\mathrm{p}{-}1) \end{bmatrix}, \tag{3.1}$$

where $\boldsymbol{X} \in \mathbb{R}^{(N_\mathrm{p}+1)n_\mathrm{x}}$ is the prediction of the future state vectors at the current time step, $\boldsymbol{U}_b \in \mathbb{R}^{N_\mathrm{p}n_\mathrm{ub}}$ and $\boldsymbol{U}_c \in \mathbb{R}^{N_\mathrm{p}}$ the future binary and continuous inputs respectively, and $\boldsymbol{V}_b \in \mathbb{R}^{N_\mathrm{p}}$ and $\boldsymbol{V}_c \in \mathbb{R}^{N_\mathrm{p}n_\mathrm{vc}}$ the prediction of the future binary and continuous disturbances. At the current time step k, the model states, inputs, and disturbances are known, so they represent a known input to the optimization problem. Furthermore, predictions of the disturbances over the horizon are inputs to the optimization problem. The prediction of the binary disturbance vector is based on a known door opening profile. The continuous disturbances in water and ambient temperature over the horizon are predicted to remain at the current measured value.

To reduce the computational effort of the optimization problem, a shorter horizon, called control horizon $N_\mathrm{c} \in \mathbb{N}_{\leq N_\mathrm{p}}$, is introduced. Only during this horizon, the control values can be freely chosen by the controller. In the remaining prediction horizon, the inputs are fixed. Further, the profile of future door openings is incorporated into the predictions only during the control horizon. During the rest of the prediction horizon, it is assumed that the door is closed. This enables the controller to track a temperature value at the end of the prediction horizon. For the same reason, the restriction on the minimum current of the TEC is also relaxed for the last sample of the control horizon and the remaining samples of the prediction horizon. The controller can thus select a current that brings the cooling chamber temperature to a set point at the end of the prediction horizon, even if the required current is below the minimum current.

Because of the two different current ranges used in the control and prediction horizon, different linearizations of the model are used for each horizon. Throughout the control horizon, the model obtained with linearization method $l = 1$ is used since this linearization approximates the nonlinear model well in the limited current range allowed in the control horizon. However, if the current is outside this narrow range, the linearization method $l = 1$ fits the nonlinear model poorly. Therefore, after the control horizon, the model obtained by the linearization method $l = 2$ is used.

In the following, the optimization problem is defined with all its constraints and its objective function.

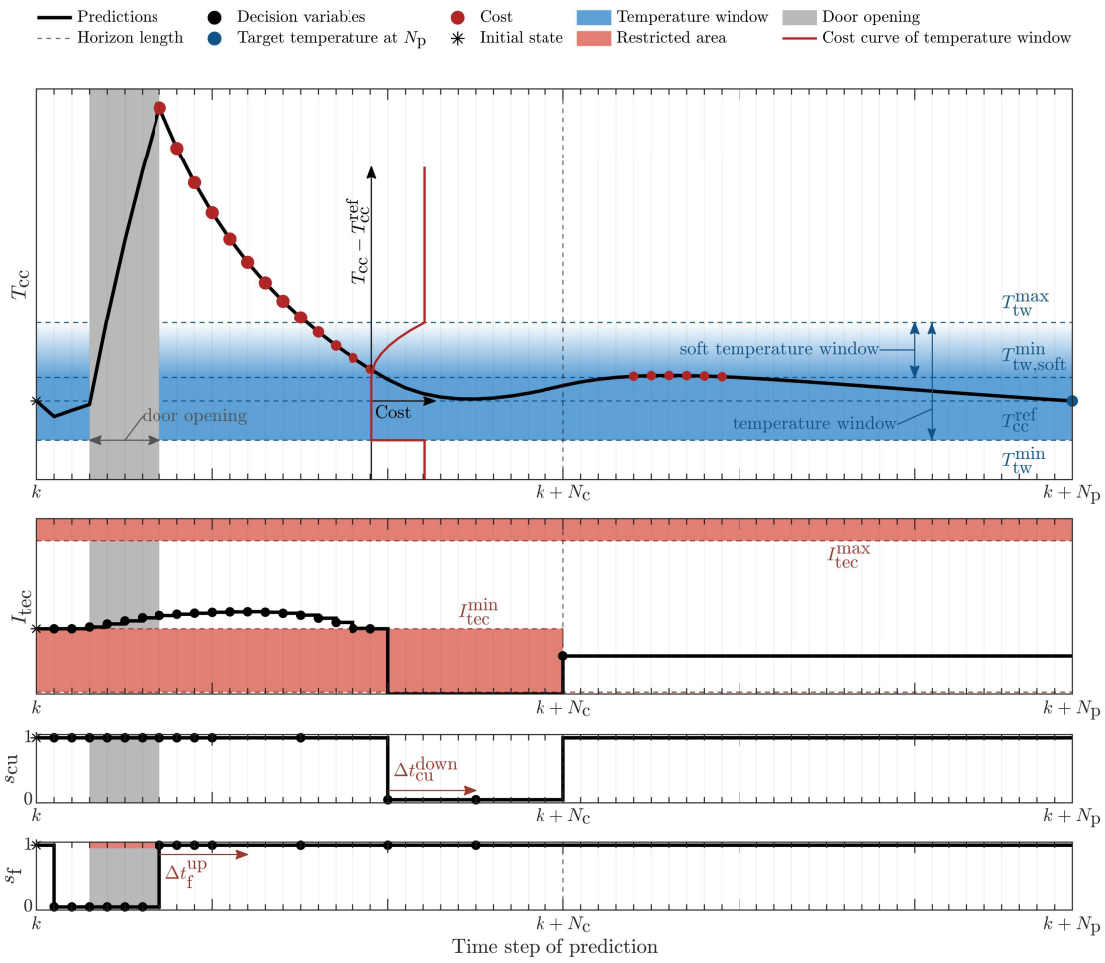

Figure 3.2: Illustration of HMPC prediction with a future door opening, highlighted by a gray background shading. The resulting costs in the objective function and the imposed constraints are depicted schematically. When the cooling chamber temperature is outside the temperature window highlighted in blue, additional costs are incurred in the objective function. The cost curve of the temperature window and the cost of the individual temperature sample are marked in red in the illustration. Furthermore, the selected future control variables of the HMPC are presented with their restrictions.

Constraints

Due to the restrictions on the plant and to reduce the computational time of solving the optimization problem, several constraints are imposed.
As explained above, the binary and continuous inputs are held at a fixed value after the control horizon till the end of the prediction horizon. The current of the TEC is held constant at the value of the last sample of the control horizon for the remainder of the prediction horizon, see (3.2a). The cooling unit and fan are always active after the control horizon to be able to track the reference temperature at the end of the prediction horizon with a constant status and to reduce the complexity of the optimization problem, yielding (3.2b) - (3.2c).

$$I_{\text{tec}}(k+i) = I_{\text{tec}}(k+N_{\text{c}}), \qquad \forall i \in \{N_{\text{c}}+1, N_{\text{c}}+2, \dots, N_{\text{p}}-1\} \tag{3.2a}$$
$$s_{\text{cu}}(k+i) = 1, \qquad \forall i \in \{N_{\text{c}}, N_{\text{c}}+1, \dots, N_{\text{p}}-1\} \tag{3.2b}$$
$$s_{\text{f}}(k+i) = 1, \qquad \forall i \in \{N_{\text{c}}, N_{\text{c}}+1, \dots, N_{\text{p}}-1\} \tag{3.2c}$$

The water and ambient temperature are assumed constant at the currently measured temperature over the whole prediction horizon, see (3.3a)-(3.3b). After the control horizon, it is predicted that the door is closed, see (3.3c).

$$T_{\text{wtr}}(k+i) = T_{\text{wtr}}(k), \qquad \forall i \in \{1, 2, \dots, N_{\text{p}}-1\} \tag{3.3a}$$
$$T_{\text{amb}}(k+i) = T_{\text{amb}}(k), \qquad \forall i \in \{1, 2, \dots, N_{\text{p}}-1\} \tag{3.3b}$$
$$s_{\text{door}}(k+i) = 0, \qquad \forall i \in \{N_{\text{c}}, N_{\text{c}}+1, \dots, N_{\text{p}}-1\} \tag{3.3c}$$

Within the control horizon, the TEC can either be operated with a current between $I_{\text{tec}}^{\min} \in \mathbb{R}_{\geq 0}$ and $I_{\text{tec}}^{\max} \in \mathbb{R}_{\geq 0}$ or with 0A, when the cooling unit is turned off. After the control horizon, the current is limited between 0A and $I_{\text{tec}}^{\max}$ to be able to maintain the cooling chamber temperature inside the temperature window since the cooling unit can not be turned off in that interval. The constraints on the continuous inputs are given by:

$$I_{\text{tec}}^{\min} s_{\text{cu}}(k+i) \leq I_{\text{tec}}(k+i) \leq I_{\text{tec}}^{\max} s_{\text{cu}}(k+i) \qquad \forall i \in \{1, 2, \dots, N_{\text{c}}-1\} \tag{3.4a}$$
$$0 \leq I_{\text{tec}}(k+i) \leq I_{\text{tec}}^{\max} \qquad \forall i \in \{N_{\text{c}}, N_{\text{c}}+1, \dots, N_{\text{p}}-1\} \tag{3.4b}$$

To fulfill the minimal up $\Delta t_{\mu}^{\text{up}} \in \mathbb{R}_{\geq 0}$ and down time $\Delta t_{\mu}^{\text{down}} \in \mathbb{R}_{\geq 0}$ of both the cooling unit and the fan, constraints similarly to those proposed in [29] are enforced:

$$s_{\mu}(k+i) - s_{\mu}(k+i\text{-}1) \leq s_{\mu}(\tau_{\text{up}}), \qquad \forall i \in \left\{-\Delta t_{\mu}^{\text{up}}, -\Delta t_{\mu}^{\text{up}}+1, \dots, N_{\text{c}}-1\right\} \tag{3.5a}$$
$$s_{\mu}(k+i\text{-}1) - s_{\mu}(k+i) \leq 1 - s_{\mu}(\tau_{\text{down}}), \qquad \forall i \in \left\{-\Delta t_{\mu}^{\text{down}}, -\Delta t_{\mu}^{\text{down}}+1, \dots, N_{\text{c}}-1\right\} \tag{3.5b}$$

with $\tau_{\text{up}} \in \{k+i, k+i+1, \dots, \min(k+N_{\text{c}}\text{-}1, k+i+\Delta t_{\mu}^{\text{up}}\text{-}1)\}$, and $\tau_{\text{down}} \in \{k+i, k+i+1, \dots, \min(k+N_{\text{c}}\text{-}1, k+i+\Delta t_{\mu}^{\text{up}}\text{-}1)\}$ and $\mu \in \{\text{cu,f}\}$.
To reduce the computation complexity of the optimization problem, the binary inputs are fixed over a certain number of time steps. The formulation of the so-called

moveblocking constraints is adopted from [30]. Instead of solving for the optimal binary inputs in the control horizon $\boldsymbol{U}_{\mathrm{b,ctr}} \coloneqq \left[\boldsymbol{u}_{\mathrm{b}}(k), \boldsymbol{u}_{\mathrm{b}}(k{+}1), \ldots, \boldsymbol{u}_{\mathrm{b}}(k{+}N_{\mathrm{c}})\right]^{\mathrm{T}} \in \mathbb{R}^{N_{\mathrm{c}} n_{\mathrm{ub}}}$ the problem is reduced to solving for the reduced binary input vector $\boldsymbol{U}^{\mathrm{red}}_{\mathrm{b,ctr}} \coloneqq \left[\boldsymbol{u}^{\mathrm{red}}_{\mathrm{b},1}, \boldsymbol{u}^{\mathrm{red}}_{\mathrm{b},2}, \ldots, \boldsymbol{u}^{\mathrm{red}}_{\mathrm{b,M}}\right]^{\mathrm{T}} \in \mathbb{R}^{M n_{\mathrm{ub}}}$ with $M \in \mathbb{N}_{\leq N_{\mathrm{c}}}$, yielding the constraint

$$\boldsymbol{U}_{\mathrm{b,ctr}} = \left(\boldsymbol{T}_{\mathrm{mb}} \otimes \boldsymbol{I}_{n_{\mathrm{ub}}}\right) \boldsymbol{U}^{\mathrm{red}}_{\mathrm{b,ctr}}, \tag{3.6}$$

where $\boldsymbol{T}_{\mathrm{mb}} \in \mathbb{R}^{(N_{\mathrm{c}}-1)\times M}$ is the blocking matrix with only zeros and ones and exactly one non-zero element in each row and $\otimes$ denotes the Kronecker product. The temperature of the heat sink is limited by $T_{\mathrm{hs,min}} \in \mathbb{R}_{\geq 0}$ to prevent excessive freezing that could damage the heat sink, yielding the constraint:

$$T_{\mathrm{hs}}(k{+}i|k) \geq T_{\mathrm{hs,min}} \qquad \forall i \in \{1, 2, \ldots, N_{\mathrm{p}}\} \tag{3.7}$$

Objective function

The objective function of the optimization problem is defined by

$$J = J_{\mathrm{P}} + J_{\mathrm{T}} + J_{\mathrm{O}} + J_{\mathrm{F}} \tag{3.8}$$

with the total cost over the horizon $J \in \mathbb{R}_{\geq 0}$, the cost of the power consumption $J_{\mathrm{P}} \in \mathbb{R}_{\geq 0}$, the cost of the deviation of the temperature window $J_{\mathrm{T}} \in \mathbb{R}_{\geq 0}$, other cost $J_{\mathrm{O}} \in \mathbb{R}_{\geq 0}$, and the terminal cost $J_{\mathrm{F}} \in \mathbb{R}_{\geq 0}$. For notational simplicity, the dependence of the objective function on the optimization variables is omitted and only explicitly stated in (3.23). The power consumption of the system comprises the power consumption of the TEC and the fan. To obtain a convex objective function, the cost of the power consumption was slightly modified, yielding

$$J_{\mathrm{P}} = \begin{cases} \sum_{i=1}^{N_{\mathrm{p}}-1} \left[I_{\mathrm{tec}}(k{+}i)\, R_1\, I_{\mathrm{tec}}(k{+}i) + R_2\, s_{\mathrm{f}}(k{+}i) \right], & \text{Normal operation} \\ 0, & \text{Pull-down operation} \end{cases} \tag{3.9}$$

with the weighting factors $R_1 \in \mathbb{R}_{\geq 0}$ and $R_2 \in \mathbb{R}_{\geq 0}$. During the initial cooling (pull-down operation), the cost of the power consumption is zero to to focus on getting into the temperature window as quickly as possible. When the temperature of the cooling chamber reaches the temperature window for the first time, the cost of the power consumption will become active (normal operation).
The temperature inside the cooling chamber should always obey a temperature window described by the minimum and maximum temperature, $T^{\mathrm{min}}_{\mathrm{tw}} \in \mathbb{R}_{\geq 0}$ and $T^{\mathrm{max}}_{\mathrm{tw}} \in \mathbb{R}_{\geq 0}$. While the door is open, the temperature window is not prescribed, because in these modes it is not feasible to realize the temperature target. The violation of the temperature window is penalized by a step cost term with the weighting factor $Q_1 \in \mathbb{R}_{\geq 0}$ in the objective function. This cost term leads to discontinuities in the objective function,

which can provoke irregular controller behavior near the boundary of the temperature window. Therefore, the discontinuity was smoothed by introducing a soft temperature window, which is only applied near the maximum temperature of the temperature window starting at $T_{\mathrm{tw,soft}}^{\mathrm{min}} \in \mathbb{R}_{\geq 0}$. The cost of the soft temperature window increases quadratically with factor $Q_2 \in \mathbb{R}_{\geq 0}$ until the cost equals the step cost at the end of the temperature window. Therefore, the cost of the temperature window can be written as follows:

$$J_{\mathrm{T}} = \sum_{i=1}^{N_{\mathrm{p}}} \Big[1 - s_{\mathrm{door}}(k{+}i)\Big] \Big[Q_1\, s_1(k{+}i|k) + s_2(k{+}i|k)\, Q_2\, s_2(k{+}i|k)\Big] \tag{3.10}$$

with the helper variables $s_1 \in \{0, 1\}$ and $s_2 \in \mathbb{R}_{\geq 0}$ to indicate if the cooling chamber temperature is outside the temperature window and to show the deviation of the temperature from the soft temperature boundary respectively, see (3.11) and (3.12).

$$s_1(k{+}i|k) = \begin{cases} 1, & \text{if } T_{\mathrm{tw}}^{\mathrm{max}} \leq T_{\mathrm{cc}}(k{+}i|k) \leq T_{\mathrm{tw}}^{\mathrm{min}} \\ 0, & \text{otherwise} \end{cases} \tag{3.11}$$

$$s_2(k{+}i|k) = \begin{cases} T_{\mathrm{cc}}(k{+}i|k) - T_{\mathrm{tw,soft}}^{\mathrm{min}}, & \text{if } T_{\mathrm{tw,soft}}^{\mathrm{min}} \leq T_{\mathrm{cc}}(k{+}i|k) \leq T_{\mathrm{tw}}^{\mathrm{max}} \\ 0, & \text{otherwise} \end{cases} \tag{3.12}$$

To obtain a continuous cost function at the maximum of the temperature window, Q_2 must satisfy the following condition:

$$Q_2 = Q_1 \left(T_{\mathrm{tw}}^{\mathrm{max}} - T_{\mathrm{tw,soft}}^{\mathrm{min}}\right)^{-2} \tag{3.13}$$

In the event of a door opening, an active fan is penalized with the weight $S \in \mathbb{R}_{\geq 0}$. These modes are very unfavorable for energy efficiency because they increase the heat transfer between the air in the cooling chamber and the ambient air. Therefore, these dynamics were not accounted for in the formulation of the model. In order for the controller to avoid these modes, high cost has been applied to them. The costs of the inefficient modes over the horizon are summarized in the following cost term:

$$J_{\mathrm{O}} = \sum_{i=1}^{N_{\mathrm{p}}-1} \Big[S\, s_{\mathrm{door}}(k{+}i)\, s_{\mathrm{f}}(k{+}i)\Big] \tag{3.14}$$

Additionally, to the costs summarized over the whole horizon, terminal costs are added to the objective function. A deviation from the reference temperature $T_{\mathrm{cc}}^{\mathrm{ref}}$ at the end of the prediction horizon is penalized with linear and quadratic cost with the weighting factors $T_1 \in \mathbb{R}_{\geq 0}$ and $T_2 \in \mathbb{R}_{\geq 0}$ respectively. Hence, the terminal costs are defined by

$$J_{\mathrm{F}} = s_3(k{+}N_{\mathrm{p}}|k)\, T_1\, s_3(k{+}N_{\mathrm{p}}|k) + T_2\, s_3(k{+}N_{\mathrm{p}}|k) \tag{3.15}$$

with the helper variable $s_3 \in \mathbb{R}$ indicating the absolute deviation from the reference temperature at the end of the prediction horizon:

$$s_3(k{+}N_{\mathrm{p}}|t) = \left|T_{\mathrm{cc}}(k{+}N_{\mathrm{p}}|k) - T_{\mathrm{cc}}^{\mathrm{ref}}\right| \tag{3.16}$$

Offset-free formulation

For a control algorithm, offset-free tracking of a reference value is essential. If the absolute value of input variables is penalized, as implemented in the proposed control scheme, offset-free control is usually not possible. However, due to the step-like cost and the much higher weighting of the violation of the temperature window compared with the input cost, the HMPC formulation still allows offset-free control.
Besides the formulation of the cost function, model inaccuracies, be it non-modeled parts or uncertainties in the model, can lead to an offset in the tracking of a reference value. To account for these unmeasured disturbances, a method proposed by [31] is adopted. The system state is augmented by $n_\mathrm{d} \in \mathbb{R}$ integrating disturbances $\boldsymbol{d} \in \mathbb{R}^{n_\mathrm{d}}$. Those disturbances are driven by a white noise $\boldsymbol{w}_\mathrm{d} \in \mathbb{R}^{n_\mathrm{d}}$, yielding

$$\boldsymbol{d}(k{+}1) = \boldsymbol{d}(k) + \boldsymbol{w}_\mathrm{d}(k). \tag{3.17}$$

The augmented system can be written as

$$\begin{aligned}\begin{bmatrix} \boldsymbol{x}(k{+}1) \\ \boldsymbol{d}(k{+}1) \end{bmatrix} = &\begin{bmatrix} \boldsymbol{A}_\mathrm{d} & \boldsymbol{\beta}_\mathrm{d} \\ \boldsymbol{0}_{n_\mathrm{d}\times n_\mathrm{x}} & \boldsymbol{I}_{n_\mathrm{d}} \end{bmatrix} \begin{bmatrix} \boldsymbol{x}(k) \\ \boldsymbol{d}(k) \end{bmatrix} + \dots \\ &\begin{bmatrix} \boldsymbol{B}_\mathrm{d} \\ \boldsymbol{0}_{n_\mathrm{d}\times n_\mathrm{u}} \end{bmatrix} u_\mathrm{c}(k) + \begin{bmatrix} \boldsymbol{E}_\mathrm{d} \\ \boldsymbol{0}_{n_\mathrm{d}\times n_\mathrm{vc}} \end{bmatrix} \boldsymbol{v}_\mathrm{c}(k) + \begin{bmatrix} \boldsymbol{g}_d \\ \boldsymbol{0}_{n_\mathrm{d}} \end{bmatrix} + \begin{bmatrix} \boldsymbol{w}_\mathrm{x}(k) \\ \boldsymbol{w}_\mathrm{d}(k) \end{bmatrix}\end{aligned} \tag{3.18a}$$

$$\begin{bmatrix} T_\mathrm{hs}(k) \\ T_\mathrm{cc}(k) \end{bmatrix} = [\boldsymbol{C}_d \ \boldsymbol{\delta}_\mathrm{d}] \begin{bmatrix} \boldsymbol{x}(k) \\ \boldsymbol{d}(k) \end{bmatrix} + \boldsymbol{D}_\mathrm{d}\, u_\mathrm{c}(k) + \boldsymbol{F}_\mathrm{d}\, \boldsymbol{v}_\mathrm{c}(k) + \boldsymbol{h}_\mathrm{d}(k) + \boldsymbol{v}_\mathrm{y}(k) \tag{3.18b}$$

with the process noise $\boldsymbol{w}_\mathrm{x} \in \mathbb{R}^{n_\mathrm{x}}$ and the measurement noise $\boldsymbol{v}_\mathrm{y} \in \mathbb{R}^2$. It should be noted that each model in the SAS and both linearization methods can have a separate disturbance model. For the sake of simplicity, in this thesis, all models use the same disturbance model. By the choice of the matrices $\boldsymbol{\beta}_\mathrm{d} \in \mathbb{R}^{n_\mathrm{x}\times n_\mathrm{d}}$ and $\boldsymbol{\delta}_\mathrm{d} \in \mathbb{R}^{2\times n_\mathrm{d}}$ the influence of the disturbances on the states and outputs is modeled. The only restriction on selecting these matrices is that the augmented system must be detectable so that an observer can estimate the states and unknown disturbances. The detectability of the system is given when the unaugmented system is detectable and the following condition holds:

$$\operatorname{rank}\left(\begin{bmatrix} \boldsymbol{I}_{n_\mathrm{x}} - \boldsymbol{A}_\mathrm{d} & -\boldsymbol{\beta}_\mathrm{d} \\ \boldsymbol{C}_d & \boldsymbol{\delta}_\mathrm{d} \end{bmatrix}\right) = n_\mathrm{x} + n_\mathrm{d} \tag{3.19}$$

Another condition follows from (3.19) and the formulation of the Kalman filter that estimates the integrating disturbance:

$$n_\mathrm{d} = n_\mathrm{y}^{fb} = 2 \tag{3.20}$$

with $n_\mathrm{y}^{fb} \in \mathbb{R}$ being the number of outputs used for feedback, which is 2 in the case of the proposed HMPC. The proof of this condition is given in [32].
To summarize, in the offset-free formulation of the HMPC, the augmented system given

in (3.18) is used by the controller to predict N_p many steps into the future. A Kalman filter, further described in Section 3.3, estimates the unknown disturbances along with the state vector.

Example 3.2.1 (Offset-free formulation):

In the following, a short illustrative example is given to clarify the offset-free formulation. For simplicity, we consider a SISO system without an integrating state with the discrete state and output equations f_x and f_y, respectively:

$$\boldsymbol{x}(k{+}1) = f_\mathrm{x}\Big(\boldsymbol{x}(k), u(k)\Big) \tag{3.21a}$$

$$y(k) = f_\mathrm{y}\Big(\boldsymbol{x}(k), u(k)\Big) \tag{3.21b}$$

Thereby, $\boldsymbol{x}$ is the state vector, u the input, and y the model output. The problem with using this unaugmented model in a model predictive control scheme is depicted in Fig. 3.3. The controller determines the future inputs so that the output trajectory $y(k{+}i|k)$ tracks the reference. However, due to the unknown disturbances acting on the system, the actual output at the next time step does not follow the predicted trajectory and remains at the same value in this example. If we now repeat the calculation of the control inputs, we get the same results. In this way, it proceeds forever, and the control system is not able to compensate for the unknown disturbances.
When the model of the controller is augmented with an integrating disturbance d, yielding

$$\boldsymbol{x}(k{+}1) = f_\mathrm{x}^\mathrm{aug}\Big(\boldsymbol{x}(k), u(k), d(k)\Big) \tag{3.22a}$$

$$y(k) = f_\mathrm{y}^\mathrm{aug}\Big(\boldsymbol{x}(k), u(k), d(k)\Big) \tag{3.22b}$$

with the augmented state and output equations $f_\mathrm{x}^\mathrm{aug}$ and $f_\mathrm{y}^\mathrm{aug}$, the controller is able to track the reference offset-free. When the output does not follow the predicted trajectory, the observer corrects for the model mismatch by adapting the estimation of the unknown disturbance and the state vector. Therefore, in the next time step, the controller determines different control variables and the predicted output trajectory should better match the actual system. This formulation allows the control scheme to compensate for the unknown disturbances and track a reference value offset-free.
Note that in this example, the control variables are instantaneously applied to the system.

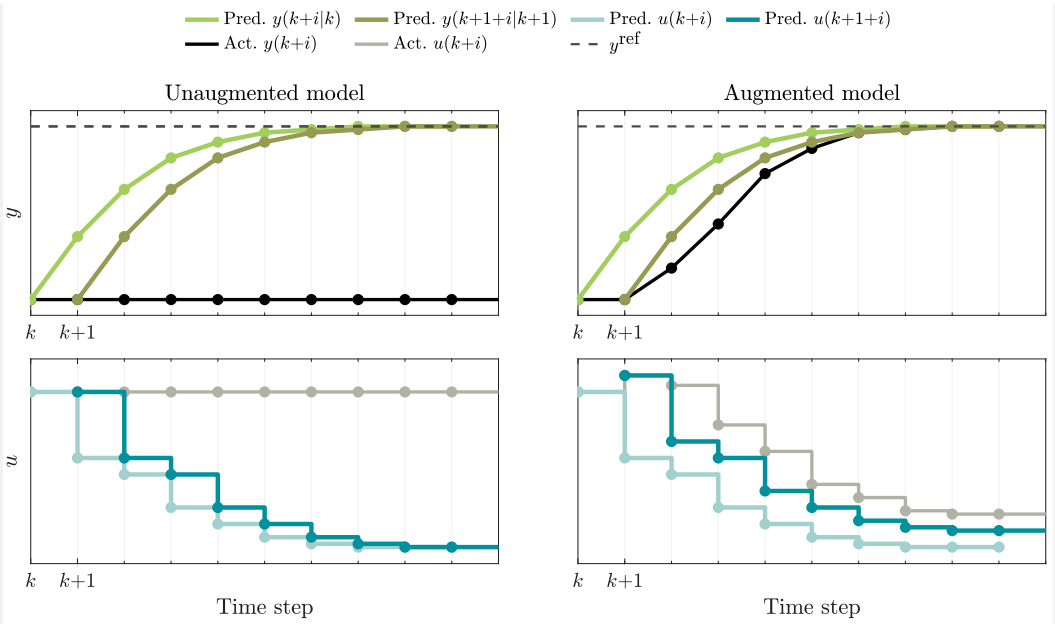

Figure 3.3: Schematic illustration of control actions using the unaugumented (left) and augmented model (right).

Implementation

Now the optimization problem can be constructed with all constraints, cost terms, and the augmented system model, yielding

$$\left[\boldsymbol{U}_{\text{b,ctr}}^{\text{red},*}, \boldsymbol{U}_{\text{c}}^{*}\right] = \underset{\boldsymbol{U}_{\text{b,ctr}}^{\text{red}}, \boldsymbol{U}_{\text{c}}}{\arg\min}\ J\left(\boldsymbol{X}, \boldsymbol{U}_{\text{b,ctr}}^{\text{red}}, \boldsymbol{U}_{\text{c}}, \boldsymbol{V}_{\text{c}}, \boldsymbol{V}_{\text{b}}\right) \tag{3.23}$$

subject to (3.2)-(3.7) and (3.18) with the optimized binary and continuous inputs, $\boldsymbol{U}_{\text{b,ctr}}^{\text{red},*}$ and $\boldsymbol{U}_{\text{c}}^{*}$ respectively, over the horizon.
However, only the optimized control variables at time step $k+1$ are implemented on the plant. In the next sample, the optimization problem is solved again to calculate the up-to-date sequence of optimized control variables, which leads to a receding horizon control law. The optimization problem is set up in Matlab using the toolbox Yalmip [33]. The Gurobi solver [34] is used to solve the optimization problem. During the tuning of the HMPC parameters special care has been taken to ensure that the HMPC can solve the optimization problem in the sampling time T_{s}.

3.2.2 Model predictive controller

To explore the advantages of the HMPC regarding its flexibility in the choice of control variables and the benefits of the model that explicitly considers door openings, a model predictive controller (MPC) with a simpler structure is proposed. This MPC also has a

hybrid model but a reduced number of modes. For easier distinction from the HMPC, this controller is referred to as MPC in the following. The MPC has almost the same formulation as the HMPC but differs in two ways. Door openings are treated not explicitly in the model formulation, but as a disturbance heat flow that directly affects the air inside the cooling chamber. Therefore, the heat transfer from the environment to the inside of the cooling chamber (2.14) is modified according to

$$\dot{Q}_{\mathrm{amb}}^{\mathrm{MPC}}(t) = \xi_1 \left[T_{\mathrm{amb}}(t) - T_{\mathrm{cc}}(t)\right] + \dot{Q}_{\mathrm{door}}^{\mathrm{MPC}}(t) \tag{3.24}$$

with the disturbance heat flow $\dot{Q}_{\mathrm{door}}^{\mathrm{MPC}} \in \mathbb{R}$ part of the continuous disturbance vector of the MPC $\boldsymbol{v}_{\mathrm{c}}^{\mathrm{MPC}}(t)$:

$$\boldsymbol{v}_{\mathrm{c}}^{\mathrm{MPC}}(t) \coloneqq \left[\; T_{\mathrm{wtr}}(t), T_{\mathrm{amb}}(t), \dot{Q}_{\mathrm{door}}^{\mathrm{MPC}}(t) \;\right]^{\mathrm{T}}. \tag{3.25}$$

The disturbance heat flow is estimated in advance based on the current temperatures and the length of the predicted door opening. The modified model makes the binary disturbance v_{b} obsolete in the formulation of MPC.
Another difference to the HMPC is that the MPC can only operate the TEC and the fan in parallel, yielding the constraint:

$$s_{\mathrm{f}}^{\mathrm{MPC}}(k{+}i) = s_{\mathrm{cu}}^{\mathrm{MPC}}(k{+}i), \qquad \forall i \in \{1, 2, \ldots, N_{\mathrm{p}}\text{-}1\} \tag{3.26}$$

These two modifications significantly reduce the number of binary decision variables in the optimization problems, which substantially shortens the computation time of the MPC compared to the HMPC.

3.2.3 PI controller

A PI controller is constructed to compare HMPC and MPC with a state-of-the-art temperature controller for refrigerated vehicles. The PI controller calculates the continuous control variable $I_{\mathrm{tec}}(k)$ based on the deviation of the measured cooling chamber temperature $T_{\mathrm{cc}}^{\mathrm{meas}} \in \mathbb{R}$ from the set point $T_{\mathrm{cc}}^{\mathrm{ref}}$. The control law is implemented in discrete-time form, yielding

$$\begin{aligned} I_{\mathrm{tec}}(k) =& I_{\mathrm{tec}}(k-1) + K_{\mathrm{p}}\left[T_{\mathrm{cc}}^{\mathrm{meas}}(k) - T_{\mathrm{cc}}^{\mathrm{ref}}\right] + \ldots \\ & K_{\mathrm{p}}\left[\frac{T_{\mathrm{s}}}{T_{\mathrm{n}}} - 1\right]\left[T_{\mathrm{cc}}^{\mathrm{meas}}(k-1) - T_{\mathrm{cc}}^{\mathrm{ref}}\right], \end{aligned} \tag{3.27}$$

with the controller parameters $K_{\mathrm{p}} \in \mathbb{R}$ and $T_{\mathrm{n}} \in \mathbb{R}$. These parameters were later tuned in simulations and experiments by the method of trial and error. Additional to this simple control law, some additional rules are imposed to comply with the restrictions on the plant (e.g minimum up and down time, ...) and to be able to set the binary control variables:

(i) **Cooling unit and fan are switched off when the current of the TEC is zero.** The PI controller sets only the single continuous control variable and does not include the other binary control variables of the plant in its formulation. Therefore, the current value set by the controller must be used to infer the state of the cooling unit and the fan. A straightforward approach has been taken, where the cooling unit and the fan are always operated in parallel. They are both switched off when the current value of the TEC is set to zero, otherwise both are active.

(ii) **Minimum up and down times are always obeyed.** It must always be ensured that minimum start-up and shut-down times of the cooling unit and the fan are observed by the temperature controller.

(iii) **The current of the TEC is set to zero when the door is opened at the next possible time step.** During a door opening, the fan should be turned off due to the increased energy consumption of that operating mode. Setting the current to zero will switch off the cooling unit and fan according to (i). However, the minimum up and down time defined by rule (ii) must always be observed.

(iv) **The current value calculated by the PI controller is limited by the minimum and maximum current.** The imposed limits of the minimum $I_{\text{tec}}^{\min}$ and maximum current $I_{\text{tec}}^{\max}$ of the plant must be observed by the temperature controller. These limits are not active when the current of the TEC is set to zero. Hence, the cooling unit and the fan are turned off.

(v) **The current of the TEC is set to zero when the temperature of the cooling chamber is below the temperature window.** Due to the restricted current range of the TEC, it is not always feasible to obey the temperature window with a constant current. Therefore, the current is set to zero and the cooling unit and fan are turned off when T_{cc} is below $T_{\text{tw}}^{\min}$. Cooling unit and fan are turned on again when T_{cc} is greater than $T_{\text{tw}}^{\max}$.

3.3 Observer

An extended Kalman filter estimates the current state $\boldsymbol{x}$ and disturbance vector $\boldsymbol{d}$, as described by [35]. The observer is necessary to overcome the lack of full-state measurability. Due to the observer's filtering of the possible noisy measurement data, the estimated values are also more favorable as inputs to the controller. The extended Kalman filter applies the nonlinear model of the plant for the estimation of both the state and the disturbance vector of the offset-free formulation. Its dynamics are determined by the process noise and measurement covariance matrix, $\boldsymbol{Q}_{\text{kf}} \in \mathbb{R}^{(n_{\text{x}}+n_{\text{d}})\times(n_{\text{x}}+n_{\text{d}})}$ and $\boldsymbol{R}_{\text{kf}} \in \mathbb{R}^{2\times 2}$ respectively. Since the process and measurement noise covariances are unknown, the specification of $\boldsymbol{Q}_{\text{kf}}$ and $\boldsymbol{R}_{\text{kf}}$ is attempted in a trial and error approach.

Chapter 4

Experimental results

In the following, the model and the controller are evaluated using an experimental setup and the results are presented and discussed. First, the experimental structure is explained in Section 4.1. Then, the model results with the identified parameters are given and the model is experimentally validated (Section 4.2). In Section 4.3, closed-loop experiments are performed with the three different temperature controllers and the results are discussed.

4.1 Experimental structure

The test bed of the cooling chamber of a small-scale refrigerated truck with a secondary loop refrigeration unit was built to evaluate the performance of the proposed temperature controllers experimentally. This test bed contains the cooling chamber, the cooling unit, and various actuators and sensors, as shown in Fig. 4.1. From the outside, the insulated walls and the door with its closing mechanism can be seen (Fig. 4.1.a). The cooling unit is located on the top of the cooling chamber with the water-cooling block on one side and the air-cooled heat sink on the other side of the TEC (Fig. 4.1.b). In Fig. 4.1.c, the inside of the cooling chamber is shown. Several temperature sensors are installed in the cooling chamber. However, only the temperature sensor on the back wall is used to measure the cooling chamber temperature $T_{\mathrm{cc}}^{\mathrm{meas}}$. An electric heater is installed at the bottom of the cooling chamber, but it was never used in the conducted experiments. The auxiliary components for the water-cooling of the cooling unit are installed at the back of the cooling chamber (Fig. 4.1.d). The most important components of the experimental setup are listed in Table 4.1.
In the following, measurement values are indicated with the superscript 'meas'.

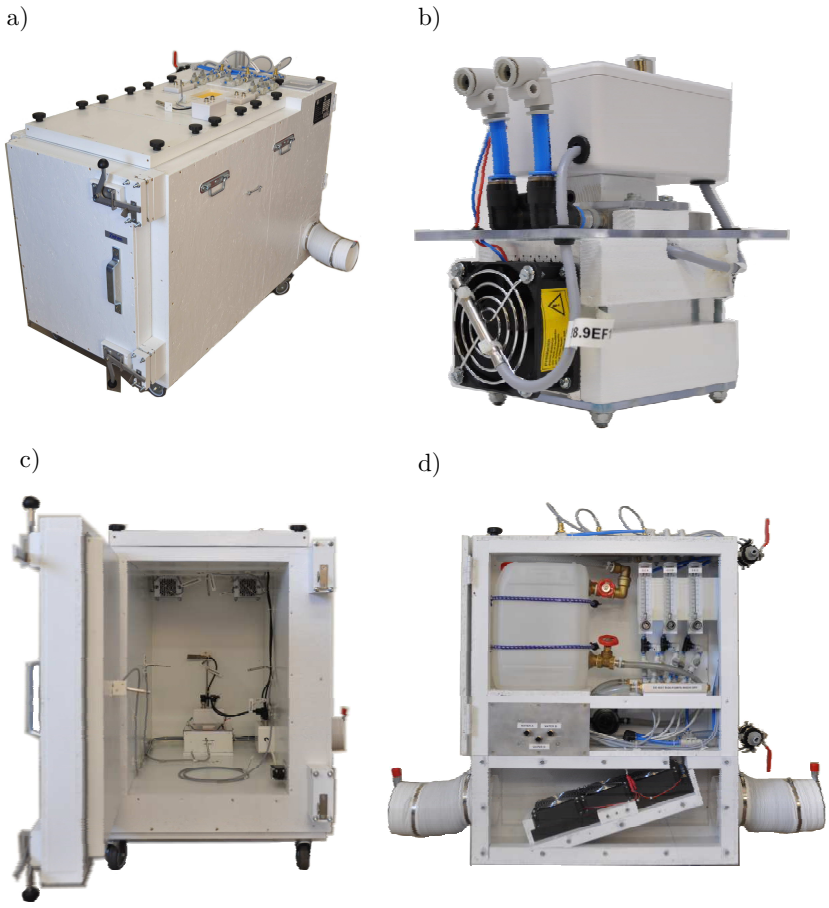

Figure 4.1: Image of cooling chamber in front view (a), cooling unit (b), inside of the cooling chamber (c), components of the water cooling at the back of the cooling chamber (d).

Table 4.1: Specifications of the experimental setup.

Condition	Value
Cooling chamber	
Dimensions	40 cm x 58.5 cm x 77 cm
Volume	180.2 liters
Cooling unit	
TEC	ET-161-12-08-E [36]
Heat Sink	Fischer LA V 6-100-24 [37]
Fan	ebmpapst 614 NHH-119 [38]
Buck-Converter	
Supply Voltage	24 V
Switching frequency	20 kHz
MOSFET	BTS7960 High Current 43 A H-Bridge Motor Driver [39]
Inductor	NAC-15-0201 [40]
Capacitor	2x in parallel THT Elektrolyt Kondensator 22 μF [41]
Diode	onsemi SB1245 [42]
Relay	Songle Relay SRD-05VDC-SL-C [43]
Data acquisition	
Sampling time $T_{\mathrm{s,meas}}$	2.5 s
Setup for $T_{\mathrm{hs}}^{\mathrm{meas}}, T_{\mathrm{cc}}^{\mathrm{meas}}, T_{\mathrm{wtr}}^{\mathrm{meas}}, T_{\mathrm{amb}}^{\mathrm{meas}}$	
Sensor	Dallas DS18B20 [44]
Accuracy	$\pm$0.5 °C
Setup for $I_{\mathrm{tec}}^{\mathrm{meas}}$	
Sensor	Texas Instruments INA260 [45]
Accuracy	$\pm$0.035 A
Setup for $P_{\mathrm{tec}}^{\mathrm{meas}}, P_{\mathrm{f}}^{\mathrm{meas}}$	
Sensor	Texas Instruments INA260 [45]
Accuracy	$\pm$3.4 W
Setup for $s_{\mathrm{door}}^{\mathrm{meas}}$	
Sensor	RS Pro AP5T31Z11 [46]

4.2 Model identification and validation

By using the methodology described in Section 2.3.2, the unknown model parameters are identified and then the model is validated. The model is trained on $n_{\mathcal{I}} = 2$ experimental data sets and evaluated on $n_{\mathcal{V}} = 1$ validation data set $\mathcal{V}$. For model identification, appropriate data acquisition is essential to measure the system behavior correctly. Uncertainties can be caused by many factors, such as sensor inaccuracies, measurement equipment, and unknown disturbances. Due to the hybrid structure of

Table 4.2: (Estimated) model parameter values.

Parameter	Normalization coefficient	(Estimated) normalized value	Unit
α_1	0.24	0.471 ($\pm$0.14%)	$\mathrm{W\,A^{-1}\,K^{-1}}$
α_2	4	0.568 ($\pm$0.02%)	$\mathrm{W\,A^{-2}}$
α_3	6	0.317 ($\pm$0.30%)	$\mathrm{W\,K^{-1}}$
β	2000	0.566 ($\pm$0.33%)	$\mathrm{W\,s\,K^{-1}}$
γ_1	12	0.609 ($\pm$0.28%)	$\mathrm{W\,K^{-1}}$
γ_2	2	0.303 ($\pm$0.50%)	$\mathrm{W\,K^{-1}}$
ζ	12	0.502 ($\pm$0.05%)	W
κ_1	15000	0.768 ($\pm$0.40%)	$\mathrm{W\,s\,K^{-1}}$
κ_2	24	0.221 ($\pm$0.67%)	$\mathrm{W\,K^{-1}}$
ξ_1	2	0.547 ($\pm$0.36%)	$\mathrm{W\,K^{-1}}$
ξ_2	60	0.257 ($\pm$0.46%)	$\mathrm{W\,K^{-1}}$
χ	8000	0.528 ($\pm$0.47%)	$\mathrm{W\,s\,K^{-1}}$

the model, it was important that the system is operated in all relevant modes in both, the identification and validation, data sets. The same applies to the continuous inputs of the system. The measurement data was collected in an open-loop fashion by mandating the controllable inputs.

Either measurement values are taken for the initial states of the model or, in case of the non-measurable wall temperature T_w, the steady state evaluation of the model is used.

By using the identification data sets, the unknown normalized parameter vector $\boldsymbol{\theta}'^*$ was estimated by applying the trust-region reflective Newton search algorithm. The normalization coefficients were chosen by an iterative procedure so that all parameters fit in the interval between 0.1 and 1. Figure 4.2 shows the estimated normalized parameters. All parameters possess a standard deviation below 0.75% of their respective mean, indicating that the model structure fits the experimental setup very well. In particular, the parameters α_2' and ζ' have a very low standard deviation, which can be explained by their static influence on the outputs of the power consumption of the TEC and the fan. This static behavior fits very well to the real conditions on the test bench and in general the electrical system can be described very well by lumped parameters. The numerical values of the parameters and their respective normalization coefficient are given in Table 4.2.

Some of the estimated parameters can be compared with the parameters specified in data sheets, which are listed in Table 4.3. Note that the TEC's data sheet parameters were converted to the parameters α_1, α_2, and α_3 used in this thesis, as described

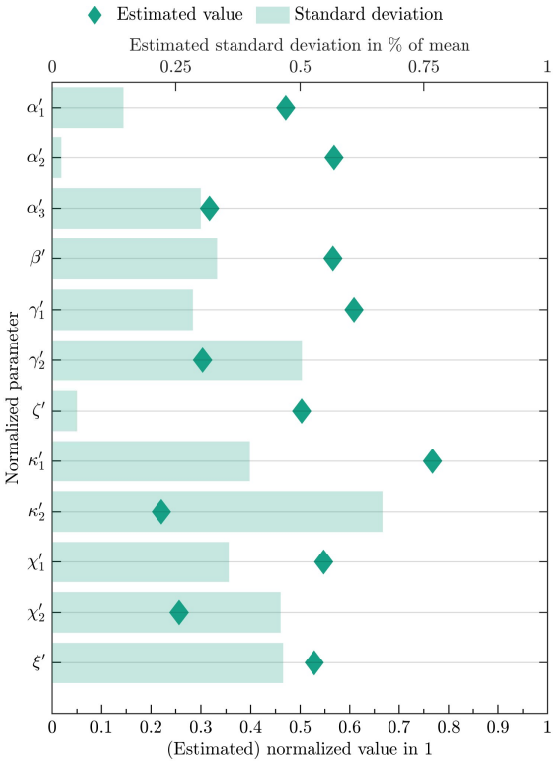

Figure 4.2: Estimated normalized values and standard deviations of model parameters. Figure adopted from [13].

in [18–20].

The estimated parameters show good agreement with those of the data sheet. The only notable deviation is in the estimated value α_2, which corresponds to the electrical resistance of the TEC. The deviation can be explained by the experimental setup having a greater resistance due to additional wires, which are not considered in the data sheet. Since the Celsius scale is much more widespread in everyday use than the Kelvin scale, temperature values will be expressed in degrees Celsius, with the conversion according to

$$\vartheta_\rho = T_\rho - 273.15 \tag{4.1}$$

with $\rho \in \{\mathrm{hs}, \mathrm{cc}, \mathrm{wall}, \mathrm{wtr}, \mathrm{amb}, \mathrm{tw}\}$.

In Fig. 4.3, the time performance of the model is evaluated using the validation data set $\mathcal{V}$ with $n_k(\mathcal{V})$ samples. Both the input and output data are presented. Due to their strong influence on the model dynamics, the two door openings are highlighted by gray background shading. The other two disturbances, ϑ_{wtr} and ϑ_{amb}, are about constant throughout the validation dataset, being 15.2 ± 0.1°C and 22.1 ± 0.2°C respectively. The controllable input of the current through the TEC is displayed in the plot at the bottom of the figure. The status of the fan and the TEC can be concluded from the related power consumption. The performance of the model can be quantitatively evaluated by

Table 4.3: (Estimated) parameter values and parameters from the data sheet

Parameter	Estimated value	Data sheet value	Unit	Difference in %
α_1	0.113	0.134 [36]	$\mathrm{W\,A^{-1}\,K^{-1}}$	15.6
α_2	5.45	3.58 [36]	$\mathrm{W\,A^{-2}}$	52.2
α_3	1.90	1.82 [36]	$\mathrm{W\,K^{-1}}$	4.4
β	1130	1026 [37]	$\mathrm{W\,s\,K^{-1}}$	10.1
ζ	6.02	5.8 [38]	W	3.8

the normalized root mean square error $\mathrm{NRMSE}_i \in \mathbb{R}$ of each output, given by

$$\mathrm{NRMSE}_i := 1 - \sqrt{\frac{\sum_{k=1}^{n_k(\mathcal{V})} y_i^{\mathrm{meas}}(t_k) - y_i(t_k)}{\sum_{k=1}^{n_k(\mathcal{V})} y_i^{\mathrm{meas}}(t_k) - \overline{y}_i^{\mathrm{meas}}}} \tag{4.2}$$

with the mean of each measured output $\overline{y}_i^{\mathrm{meas}} \in \mathbb{R}$ according to

$$\overline{y}_i^{\mathrm{meas}} = \sum_{k=1}^{n_k(\mathcal{V})} y_i^{\mathrm{meas}}(t_k), \tag{4.3}$$

and the subscript i indicating the respective output. From a purely visual point of view, the model outputs correspond very well to measurement data. This is also quantitatively supported by the high values of the NRMSE. Especially the model outputs of the heat sink temperature, ϑ_{hs}, and the power consumption of the TEC, P_{tec}, have an excellent fit to the validation data. The model output of the cooling chamber temperature, ϑ_{cc}, has the lowest NRMSE of all outputs and also deviates noticeably from the measurements, particularly in the event of a door opening. The relatively simple model for a door opening and subsequent cooling by the stored thermal energy in the wall and heat sink has difficulty describing these complex dynamics because the dynamics on the test bench are additionally influenced by other factors such as humidity and air flow through the cooling chamber that are not explicitly considered in the model. In general, however, the fit is very good even on this output, especially considering the low order of the model. The power consumption of the fan, P_{f}, is also well represented by the model. The noisy measurements explain the relatively low NRMSE of only 77.5% on this output, which is due to the limited accuracy of the sensor in low power ranges.
To be able to bring the model into the chosen DHA formulation, the system is linearized according to Section 2.3.3. Two different linearizations were conducted, $l = 1$ and $l = 2$. The first linearization is valid only in a very restricted current interval, while the second

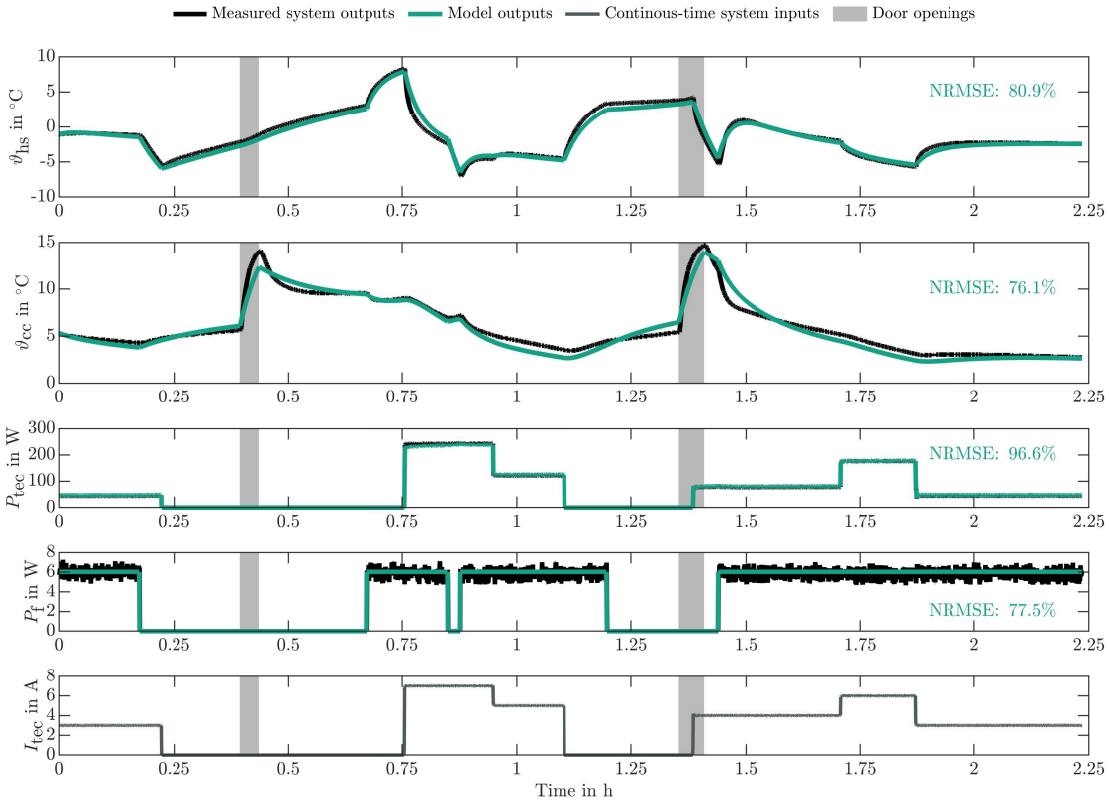

Figure 4.3: Comparison of experimentally obtained measurement data and model outputs on validation data set $\mathcal{V}$. In the first two graphs, the heat sink and cooling chamber temperature are displayed, followed by the power consumption of the TEC and the fan. At the bottom of the figure, the current of the TEC is plotted. The respective power consumption can be used to infer the status of the cooling unit and the fan. Door openings are indicated by gray background shading, while the other measurable disturbances of the system are constant over time at $\vartheta_{\text{wtr}} = 15.2 \pm 0.1°\text{C}$ and $\vartheta_{\text{amb}} = 22.1 \pm 0.2°\text{C}$. Furthermore, the NRMSE is given for the respective outputs.

should provide a good fit in a wider current range. The linearization parameters were fitted to the nonlinear model in a limited current and heat sink temperature range. The selected intervals and the fitted parameters are depicted in Table 4.4.

Table 4.4: Fitted linearization parameters

	Linearization $l = 1$	Linearization $l = 2$
Fitting Intervals		
$I_{\text{tec}}^{\text{lin,min}}$	3A	0A
$I_{\text{tec}}^{\text{lin,max}}$	7A	7A
$\vartheta_{\text{hs}}^{\text{lin,min}}$	-7.5°C	-7.5°C
$\vartheta_{\text{hs}}^{\text{lin,max}}$	17.5°C	17.5°C
Fitted Parameters		
λ_1	$0.5646\,\text{W}\,\text{K}^{-1}$	-
λ_2	$8.684\,\text{W}\,\text{A}^{-1}$	-
λ_3	-103.4W	-
λ_4	-	$19.39\,\text{W}\,\text{A}^{-1}$

4.3 Controller performance

First, the parameters of the controller and the observer are tuned. Care was taken to ensure that the controllers have similar dynamics to be comparable. The results of the tuned parameters of the controllers and the observer are displayed in Table 4.5. The blocking matrix T_{mb} is presented separately in Table 4.6.
The performance of the three controllers was evaluated on a 5.25 hours experiment with four door openings, shown in Fig. 4.4. The two predictive controllers knew those four door openings in advance and incorporated them into their predictions. The experiment was divided in four intervals $\mathcal{S}_j, j \in \{1, 2, 3, 4\}$ with $n_k(\mathcal{S}_j)$ samples each, to evaluate each controller in those intervals. The first interval $\mathcal{S}_1$ has a total length of 1.5 hours, during which the cooling chamber temperature is cooled down from ambient temperature to the reference temperature. It should be noted that during this pull-down operation, the HMPC and MPC have a different objective function that does not take the power consumption into account compared to the normal operation as described in Section 3.2.1. The remaining 3.75 hours of the experiment were divided into three intervals of equal length. Interval $\mathcal{S}_2$ has a single door opening with a duration of 3 minutes, starting 2 hours after the start of the experiment. The next two door openings are included in the third interval $\mathcal{S}_3$. The second door opening starts at 3 hours with a duration of 2 minutes, shortly followed by the third door opening at 3 hours and 5 minutes with a duration of 2 minutes as well. The last interval $\mathcal{S}_4$ has a long door

Table 4.5: Tuned parameter values of controllers and observer

Parameter	Value	Unit
T_s	20	s
N_p	1200	s
N_c	620	s
$I_\mathrm{tec}^\mathrm{min}$	3	A
$I_\mathrm{tec}^\mathrm{max}$	7	A
$\Delta t_\mathrm{cu}^\mathrm{up}$	100	s
$\Delta t_\mathrm{cu}^\mathrm{down}$	100	s
$\Delta t_\mathrm{f}^\mathrm{up}$	100	s
$\Delta t_\mathrm{f}^\mathrm{down}$	100	s
$\vartheta_\mathrm{hs,min}$	-10	°C
$\vartheta_\mathrm{tw}^\mathrm{min}$	4.5	°C
$\vartheta_\mathrm{tw}^\mathrm{max}$	5.5	°C
$\vartheta_\mathrm{tw,soft}^\mathrm{min}$	5.3	°C
$\vartheta_\mathrm{cc}^\mathrm{ref}$	5	°C

Parameter	Value	Unit
R_1	11.361	-
R_2	30.169	-
Q_1	400	-
Q_2	10000	-
S	1000	-
T_1	1000	-
T_2	5000	-
$\boldsymbol{\beta}_\mathrm{d}$	$0_{3\times2}$	-
$\boldsymbol{\delta}_\mathrm{d}$	I_2	-
K_p	-2	-
T_n	200	-
$\boldsymbol{Q}_\mathrm{kf}$	diag $[1, 1, 0.01, 1, 1]$	-
$\boldsymbol{R}_\mathrm{kf}$	I_2	-

Table 4.6: Blocking matrix T_mb of HMPC and MPC

Row	1	2	3	4	5	6	7	8	9	10	11	12	13	14	15
Column	1	2	3	4	5	6	7	8	9	10	11	11	11	11	11
Value	1	1	1	1	1	1	1	1	1	1	1	1	1	1	1
Row	16	17	18	19	20	21	22	23	24	25	26	27	28	29	30
Column	12	12	12	12	12	13	13	13	13	13	13	13	13	13	13
Value	1	1	1	1	1	1	1	1	1	1	1	1	1	1	1

opening (=5 minutes) at 4 hours and 20 minutes after the start of the experiment. This experiment was repeated for the three different controllers. Care was taken to ensure that the water temperature of the water-cooling and the ambient conditions were the same for all controllers.

The water ($=15.4 \pm 0.2$°C) and ambient temperature ($=22.0 \pm 0.2$°C) were constant throughout the experiment with all three controllers. Without door openings, it is clearly visible that all three controllers are able to fulfill the temperature window. Moreover, each of the controllers is able to cool down the temperature of the cooling chamber in a reasonable time after a door opening. However, the total power consumption $P_\mathrm{total}^{meas} = P_\mathrm{tec}^\mathrm{meas} + P_\mathrm{f}^\mathrm{meas} \in \mathbb{R}$ differs significantly among the three controllers. This results in energy savings with the two predictive controllers compared to the state-of-the-art PI controller. The relative energy savings $E_\mathrm{saving} \in \mathbb{R}$ of each controller

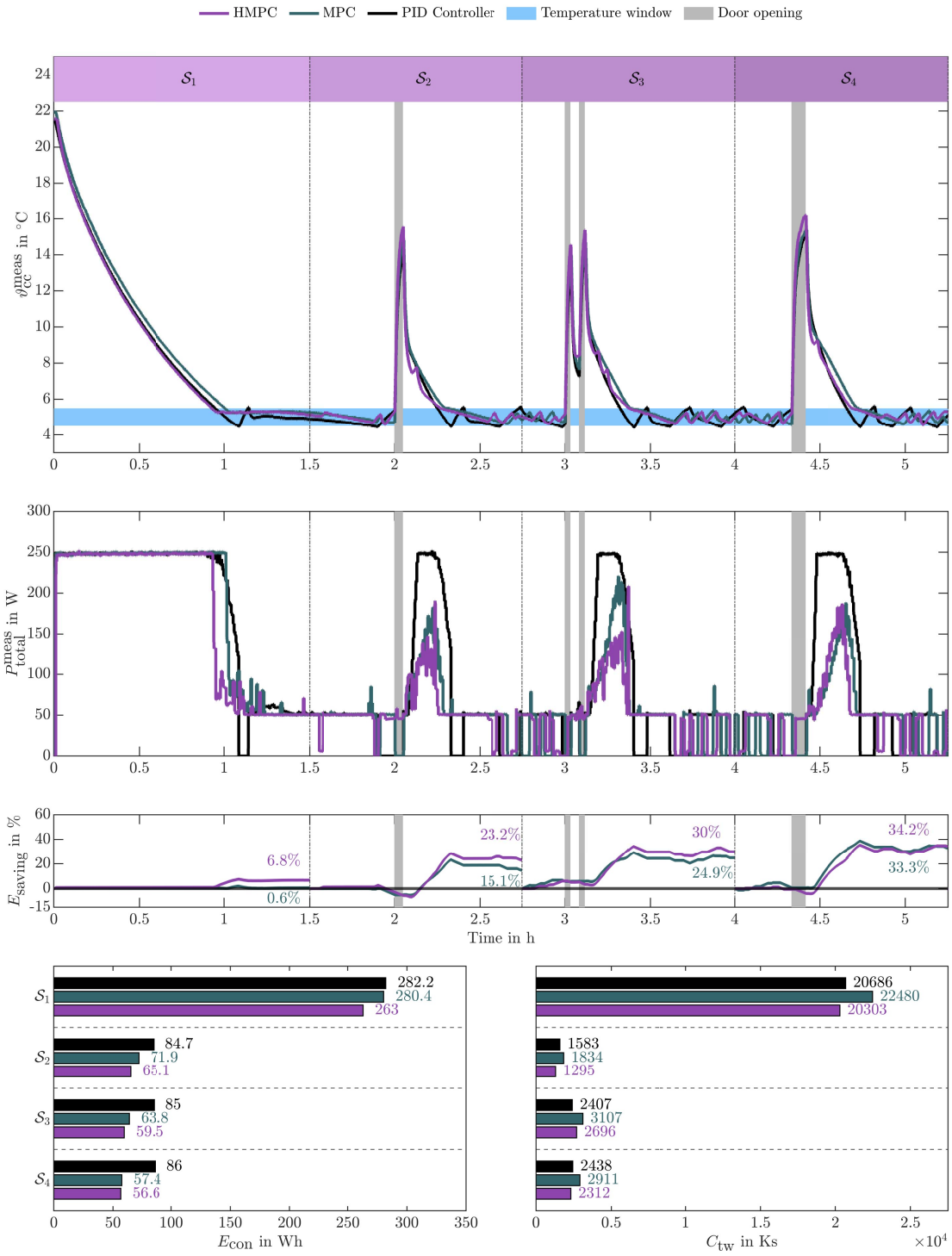

Figure 4.4: Experimental evaluation of the three temperature controllers. The closed-loop experiment with four door openings is divided into four intervals. The three upper diagrams depict the cooling chamber temperature, the total power consumption, and the energy savings in each interval over time. The bar graphs at the bottom show the total energy consumption E_{con} and the right Riemann sum of the temperature window violation in each interval C_{tw}, respectively.

compared to the PI controller in each interval are defined according to

$$E_{\text{saving}}(k, \mathcal{S}_j, ctr) = T_{\text{s,meas}} \frac{\sum_{k=1}^{k} \left[P_{\text{total}}^{\text{meas}}(k, \text{PI}) - P_{\text{total}}^{\text{meas}}(k, ctr) \right]}{\sum_{k=1}^{k} P_{\text{total}}^{\text{meas}}(k, \text{PI})} \tag{4.4}$$

with $ctr \in \{\text{HMPC}, \text{MPC}, \text{PI}\}$ indicating the controller configuration.
The bar graph at the bottom left of Fig. 4.4 shows the total energy consumption $E_{\text{con}} \in \mathbb{R}$ according to

$$E_{\text{con}}(\mathcal{S}_j, ctr) = T_{\text{s,meas}} \sum_{k=1}^{n_k(\mathcal{S}_j)} P_{\text{total}}^{\text{meas}}(k, ctr). \tag{4.5}$$

The other bar graph shows the right Riemann sum of the temperature window violation $C_{\text{tw}} \in \mathbb{R}$ without the intervals of the door openings according to

$$C_{\text{tw}}(\mathcal{S}_j, ctr) = T_{\text{s,meas}} \sum_{k=1}^{n_k(\mathcal{S}_j)} \begin{cases} T_{\text{cc}}^{\text{meas}}(k) - T_{\text{tw}}^{\max}, & \text{if } T_{\text{cc}}^{\text{meas}}(k) \geq T_{\text{tw}}^{\max} \wedge s_{\text{door}}^{\text{meas}}(k) = 0 \\ T_{\text{tw}}^{\min} - T_{\text{cc}}^{\text{meas}}(k), & \text{if } T_{\text{cc}}^{\text{meas}}(k) \leq T_{\text{tw}}^{\min} \wedge s_{\text{door}}^{\text{meas}}(k) = 0 \\ 0, & \text{otherwise} \end{cases}. \tag{4.6}$$

In interval $\mathcal{S}_1$, the performance of the three controllers is almost identical. During the pull-down operation, all three controllers operate with maximum power consumption to cool down the cooling chamber as quickly as possible. Only small energy savings are achievable for the HMPC and MPC by reducing the power consumption slightly earlier than the PI controller. The HMPC and PI controller comply with the temperature restrictions better than the MPC, as shown by the loweer C_{tw} values. However, the energy savings and the C_{tw} value in this interval are strongly dependent on the initial conditions of the system. In the second interval $\mathcal{S}_2$, the HMPC is able to save 23.2% of energy compared with the PI controller and at the same time maintain the temperature window better. The MPC can also save 15.1% in this interval but cools down the cooling chamber after the door opening significantly slower than the MPC and PI controller. The same applies to interval $\mathcal{S}_3$ and $\mathcal{S}_4$ with energy saving with the HMPC of 30% and 34% and with the MPC of 24.9% and 33.3% compared with the PI controller. In $\mathcal{S}_3$, the PI controller has the best performance regarding the indicator C_{tw} for the violation of the temperature window. That can be explained by the increased cooling of the PI controller between the two door openings. However, this behavior is very inefficient since the door is opened again and the cold air is lost to the environment. Therefore, the two predictive controllers, knowing the next door opening, reduce their cooling capacity between the successive door openings. Overall, the HMPC saves 17.4% energy over the entire 5.25 hour experiment, while the MPC saves 12.0% compared with the PI controller.
Since door openings of refrigerated trucks are not always precisely known, the three controllers are evaluated on another experiment $\mathcal{S}_5$ with an unexpected door open-

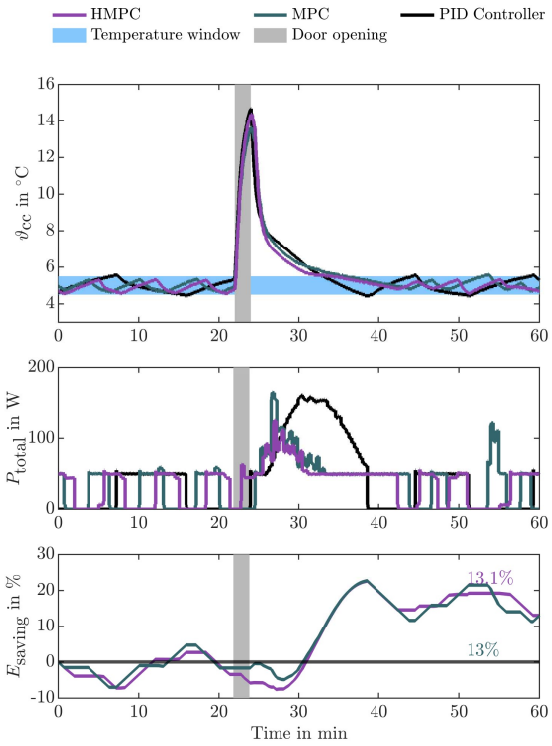

Figure 4.5: Controller evaluation on experiment $\mathcal{S}_5$ with an unexpected door opening. The temperature of the cooling chamber, the total power consumption, and the energy savings are plotted over time. Furthermore, the unanticipated door opening is indicated by a gray background shading. The water temperature and ambient temperature were constant throughout the experiment at 15.3 ± 0.1°C and 21.7 ± 0.1°C respectively.

ing with a duration of two minutes. The two predictive controllers have no information about the door opening during this interval, and only when the door opens, the HMPC and MPC assume that the door will remain open for another two minutes. This predicted door opening interval is shifted forward until the door is closed again. In Fig. 4.5 the results of the experiment with the unexpected door opening are shown. Both water temperature and ambient temperature were again constant for all three controllers at 15.3 ± 0.1°C and 21.7 ± 0.1°C, respectively. As in the previous experiment, the two predictive controllers can achieve lower energy consumption than the PI controller. The total power consumption with the HMPC and MPC is 35.0Wh and 35.1Wh respectively, and with the PI controller is 40.3Wh, yielding energy savings of 13.1% and 13.0% for the HMPC and MPC compared with the PI controller. Though the performance of the MPC in terms of observing the temperature window is significantly worse compared with the HMPC and PI controller ($C_{tw}(\mathcal{S}_5, \text{HMPC}) = 985\,\text{Ks}$, $C_{tw}(\mathcal{S}_5, \text{MPC}) = 1115\,\text{Ks}$, $C_{tw}(\mathcal{S}_5, \text{PI}) = 1073\,\text{Ks}$).

In general, it can be said that the two predictive controllers achieve the largest energy savings when a door opening occurs. The two predictive controllers can save energy by storing thermal energy in the cooling unit's secondary loop prior to the expected door opening and quickly releasing it to the air inside cooling chambers after the door is closed. This allows the predictive controllers to reduce the cooling capacity after the door is closed, thereby operating the cooling unit more efficiently while achieving the same cooling of the air after the door is closed as with the PI controller. During the pull-down operation the HMPC is able to achieve energy saving of 6.8% by reducing the cooling capacity earlier than the PI controller. The MPC only achieves marginal savings of 0.6%.
Furthermore, the computing time of the individual controllers must be considered. The HMPC needs by far the longest time for the calculation of the controlled variables, and occasionally reaches the limit of the sampling time. When the sampling time is exceeded, a suboptimal solution is applied by the HMPC. The MPC and PI controller require significantly less computing time to determine the control variables and never come close to the limit of the sampling time.
Nevertheless, the experimental results show that the proposed HMPC can outperform the other two controllers in terms of compliance to temperature requirements and achieving high overall energy efficiency. The MPC may also achieve similar energy savings as the HMPC compared to a state-of-the-art PI controller. However, it performed the worst out of the three controllers in terms of maintaining the temperature window. Adjusting the MPC's weighting parameters may improve performance in terms of maintaining the temperature window, but this would also result in increased energy consumption of the MPC.

Chapter 5

Discussion

The proposed HMPC shows exceptional results in meeting temperature restrictions while achieving high overall energy efficiency. With respect to both objectives, the HMPC has a significantly better performance than the other two controllers used for comparison.

The advantages of the HMPC may be further enhanced by expanding the horizons and generally relaxing some of the constraints imposed to reduce the computational time of the controller. These restrictions to the optimization problem reduce the search space of the optimizer, and more optimal solutions may be excluded. However, for the real-time implementation of the controller on the experimental setup, these constraints were necessary to find a solution of the optimization problem within the sampling time of the controller.

While all controllers observe the minimum startup and shutdown times, it is apparent that the two model-based controllers turn the cooling unit and fan on or off much more frequently than the PI controller. The wear of the cooling unit's compressor depends mainly on the on-off cycles. Hence the number of cycles should be kept as low as possible to increase the lifetime of the cooling unit. For this reason, others [47] explicitly considered the switching event in the objective function of the control scheme.

Direct control of the cargo temperature instead of regulating the air temperature inside the cooling chamber would have obvious advantages. In the literature several authors proposed models for estimating the cargo temperature [48–50]. However, for these models, accurate estimates of the cargo properties are necessary. In case the same goods are repeatedly transported, the parameters of the goods could be estimated and the model of the cargo could be integrated into the controller formulation. The additional effort could be justified for transporting pharmaceutical products, which are costly and subject to strict temperature restrictions.

The studies performed are limited to temperatures above the freezing point. However, many refrigeration applications operate well below these temperatures, necessitating the inclusion of mass infiltration and air humidity in the model formulation [51, 52]. Another aspect that must be considered in the model with temperatures below the freezing point is the formation of frost on the components inside the cooling cham-

ber [53]. Frost can significantly reduce the cooling capacity and also increase energy consumption, so a suitable strategy for defrosting should be considered in the control scheme [54].
The model of the cooling chamber and cooling unit shows highly satisfactory results on the experimental setup, especially when considering the low order of the model, which is very beneficial for real-time control applications to reduce computational time. However, the model neglects some environmental factors that could affect the performance of an actual refrigerated vehicle on the road, such as thermal radiation, vehicle speed, and air humidity. Those influences could be subject to further research.

Chapter 6

Conclusion

This work introduces a model predictive control scheme for a refrigerated truck with a secondary loop cooling unit to control the air temperature inside its cooling chamber. Experimental closed-loop results show that an advanced control scheme can achieve energy savings compared to less sophisticated controllers while maintaining temperature requirements by taking full advantage of the flexibility of the secondary refrigeration unit. The benefits of the sophisticated control concept are particularly evident when the door of the cooling chamber is opened, resulting in energy savings of up to 34.2% during a single door opening compared with a state-of-the-art PI temperature controller with similar performance in meeting the temperature requirements. During a 5.25 hour long experiment, the advanced control concept consumed 17.4% less electrical energy than the PI controller. The advantages of flexibility in the selection of control variables and the explicit consideration of door openings are also apparent when compared to another model-based predictive control concept.

The predictive control scheme relies on a dynamic model of the system, which has an excellent fit on the experimental setup considering the low order of the model. In the validation experiment, the important model outputs for the cooling chamber temperature and the power consumption of the TEC have an NRMSE of 76.1% and 96.6%, respectively.

For a small-scale refrigerated truck under consideration, it can be justified that some influences have been neglected in this thesis, such as solar radiation, vehicle speed, cargo temperature, and frost formation. However, the results show that for a refrigerated truck with a secondary loop refrigeration system, energy efficiency and compliance with temperature requirements can be significantly improved with sophisticated predictive control schemes.

Bibliography

[1] Cold chain market size, share trends analysis report by type (storage, monitoring components), by equipment (storage, transportation), by application (fish, meat seafood), by packaging, and segment forecasts, 2021 - 2028. `https://www.grandviewresearch.com/industry-analysis/cold-chain-market`. Accessed: 2022-09-27.

[2] Lisa Kitinoja. Use of cold chains for reducing food losses in developing countries. *Population*, 6(1.23):5–60, 2013.

[3] Reiner Jedermann, Ulrike Praeger, Martin Geyer Leibniz, and Walter Lang. Temperature deviations during transport as a cause for food losses. In *Preventing food losses and waste to achieve food security and sustainability*, pages 301–340. Burleigh Dodds Science Publishing, 2020.

[4] The cost of a broken cold chain in the pharmaceutical industry. `https://pharma-mon.com/drug-storage-monitoring/the-cost-of-a-broken-cold-chain-in-the-pharmaceutical-industry/`. Accessed: 2022-09-27.

[5] SJ James, C James, and JA Evans. Modelling of food transportation systems–a review. *International Journal of Refrigeration*, 29(6):947–957, 2006.

[6] Oludaisi Adekomaya, Tamba Jamiru, Rotimi Sadiku, and Zhongjie Huan. Sustaining the shelf life of fresh food in cold chain–a burden on the environment. *Alexandria Engineering Journal*, 55(2):1359–1365, 2016.

[7] Seyed Ehsan Shafiei and Andrew Alleyne. Model predictive control of hybrid thermal energy systems in transport refrigeration. *Applied Thermal Engineering*, 82:264–280, 2015.

[8] Kresten K Sørensen, Jakob Stoustrup, and Thomas Bak. Adaptive mpc for a reefer container. *Control Engineering Practice*, 44:55–64, 2015.

[9] Elisabeth Luchini, Dominik Radler, Daniel Ritzberger, Stefan Jakubek, and Martin Kozek. Model predictive temperature control and ageing estimation for an insulated cool box. *Applied Thermal Engineering*, 144:269–277, 2018.

[10] Elisabeth Luchini, Agnes Poks, Dominik Radler, and Martin Kozek. Model predictive temperature control for a food transporter with door-openings. In *2020 SICE International Symposium on Control Systems (SICE ISCS)*, pages 85–91. IEEE, 2020.

[11] Kai Wang, Magnus Eisele, Yunho Hwang, and Reinhard Radermacher. Review of secondary loop refrigeration systems. *International Journal of Refrigeration*, 33(2):212–234, 2010.

[12] Joseph Fasl. Modeling and control of hybrid vapor compression cycles. 2013.

[13] Markus Fallmann, Agnes Poks, and Martin Kozek. Control-oriented hybrid model of a small-scale refrigerated truck chamber. *Submitted to Applied Thermal Engineering, unpublished.*

[14] Markus Fallmann, Julian Kölbl, Tobias Ausweger, Maximilian Lösch, Agnes Poks, and Martin Kozek. Emulation of refrigeration units by peltier elements: An impedance control approach. *unpublished.*

[15] T Seetawan, U Seetawan, A Ratchasin, S Srichai, K Singsoog, W Namhongsa, C Ruttanapun, and S Siridejachai. Analysis of thermoelectric generator by finite element method. *Procedia Engineering*, 32:1006–1011, 2012.

[16] Khaled Teffah, Youtong Zhang, and Xiao-long Mou. Modeling and experimentation of new thermoelectric cooler–thermoelectric generator module. *Energies*, 11(3):576, 2018.

[17] Dongliang Zhao and Gang Tan. A review of thermoelectric cooling: materials, modeling and applications. *Applied thermal engineering*, 66(1-2):15–24, 2014.

[18] Gianluca A Mannella, Vincenzo La Carrubba, and Valerio Brucato. Peltier cells as temperature control elements: Experimental characterization and modeling. *Applied thermal engineering*, 63(1):234–245, 2014.

[19] HY Zhang, YC Mui, and M Tarin. Analysis of thermoelectric cooler performance for high power electronic packages. *Applied thermal engineering*, 30(6-7):561–568, 2010.

[20] Simon Lineykin and Shmuel Ben-Yaakov. Modeling and analysis of thermoelectric modules. *IEEE Transactions on Industry Applications*, 43(2):505–512, 2007.

[21] G Fraisse, J Ramousse, D Sgorlon, and C Goupil. Comparison of different modeling approaches for thermoelectric elements. *Energy conversion and management*, 65:351–356, 2013.

[22] MA Ben Taher, M Mahdaoui, T Kousksou, Y Zeraouli, and M Ahachad. Numerical study of the aero-thermal performance for different scenarios of a refrigerated truck using urans. *Journal of Cleaner Production*, 320:128775, 2021.

[23] T Lafaye De Micheaux, M Ducoulombier, Jean Moureh, V Sartre, and J Bonjour. Experimental and numerical investigation of the infiltration heat load during the opening of a refrigerated truck body. *International Journal of Refrigeration*, 54:170–189, 2015.

[24] Paolo Artuso, Antonio Rossetti, Silvia Minetto, Sergio Marinetti, Lorenzo Moro, and Davide Del Col. Dynamic modeling and thermal performance analysis of a refrigerated truck body during operation. *International Journal of Refrigeration*, 99:288–299, 2019.

[25] Francesco Borrelli, Alberto Bemporad, and Manfred Morari. *Predictive control for linear and hybrid systems*. Cambridge University Press, 2017.

[26] Renny Rakhmawati, Janitra Hilmyvarafi Farrasbyan, Farid Dwi Murdianto, et al. Performance robustness of pid controller in buck converter for cooling system. In *2018 International Seminar on Application for Technology of Information and Communication*, pages 127–132. IEEE, 2018.

[27] Şerban Mihalache, Irina Flamaropol, Florin-Silviu Dumitru, Lidia Dobrescu, and Dragoş Dobrescu. Automated cooling control system through peltier effect and high efficiency control using a dc-dc buck converter. In *2015 International Semiconductor Conference (CAS)*, pages 281–284. IEEE, 2015.

[28] Jean-Paul Rodrigue. *The geography of transport systems*. Routledge, 2020.

[29] Barbara Mayer, Michaela Killian, and Martin Kozek. Management of hybrid energy supply systems in buildings using mixed-integer model predictive control. *Energy conversion and management*, 98:470–483, 2015.

[30] Raphael Cagienard, Pascal Grieder, Eric C Kerrigan, and Manfred Morari. Move blocking strategies in receding horizon control. *Journal of Process Control*, 17(6):563–570, 2007.

[31] James Blake Rawlings, David Q Mayne, and Moritz Diehl. *Model predictive control: theory, computation, and design*, volume 2. Nob Hill Publishing Madison, WI, 2017.

[32] Gabriele Pannocchia and James B Rawlings. Disturbance models for offset-free model-predictive control. *AIChE journal*, 49(2):426–437, 2003.

[33] J. Löfberg. Yalmip : A toolbox for modeling and optimization in matlab. In *In Proceedings of the CACSD Conference*, Taipei, Taiwan, 2004.

[34] Gurobi Optimization, LLC. Gurobi Optimizer Reference Manual, 2022.

[35] D. Simon. *Nonlinear Kalman filtering*, chapter 13, pages 393–431. John Wiley Sons, Ltd, 2006.

[36] Datasheet: ET-161-12-08-E. https://de.rs-online.com/web/p/peltiermodule/6935107. European Thermodynamics GmbH, Kibworth, United Kingdom, Accessed: 2022-09-22.

[37] Datasheet: LA V 6 100 24. https://www.fischerelektronik.at/web_fischer/en_GB/cool/D04/Cooling%20aggregates%20with%20axial%20fan/PR/LA_V6_/index.xhtml. Fischer Elektronik GmbH Co. KG, St.Georgen , Austria, Accessed: 2022-09-22.

[38] Datasheet: ebmpapst 614 NHH-119. https://www.fischerelektronik.at/web_fischer/en_GB/cool/D04/Cooling0aggregates0with0axial0fan/PR/LA_V6_/index.xhtml. ebm-papst St.Georgen GmbH Co. KG, Lüdenscheid, Germany, Accessed: 2022-09-22.

[39] Datasheet: BTS7960 High Current 43A H-Bridge Motor Driver. http://handsontec.com/index.php/product/43a-high-power-bts7960-dc-motor-driver-module/. Handson Technology Enterprise, Johor, Malaysia, Accessed: 2022-09-24.

[40] Datasheet: NAC-15-0201. https://at.rs-online.com. RS Group plc, London, United Kingdom, Accessed: 2022-09-24.

[41] Datasheet: THT Elektrolyt Kondensator 22F. https://at.rs-online.com. RS Group plc, London, United Kingdom, Accessed: 2022-09-24.

[42] Datasheet: onsemi SB1245. https://at.rs-online.com. RS Group plc, London, United Kingdom, Accessed: 2022-09-24.

[43] Datasheet: RS-Pro SRD-05VDC-SL-C. https://www.circuitbasics.com/wp-content/uploads/2015/11/SRD-05VDC-SL-C-Datasheet.pdf. Ningbo Songle Relay Co.,ltd., Zhejiang, China, Accessed: 2022-09-22.

[44] Datasheet: Dallas DS18S20. https://www.sensorshop24.de/kabelfuehler-durchmesser-6mm. otom Group GmbH, Bräunlingen, Germany, Accessed: 2022-09-22.

[45] Datasheet: Texas Instruments INA260. https://www.ti.com/product/INA260#params. Texas Instruments Incorporated, Dallas, United States of America, Accessed: 2022-09-22.

[46] Datasheet: RS-Pro AP5T31Z11. https://docs.rs-online.com/a5b5/0900766b81567448.pdf. RS Group plc, London, United Kingdom, Accessed: 2022-09-22.

[47] Elisabeth Luchini, Filip Kitanoski, and Martin Kozek. Multi-objective optimization of the operational modes for redundant refrigeration circuits. *Applied Thermal Engineering*, 122:409–419, 2017.

[48] AH Raval, SC Solanki, and Rajvir Yadav. A simplified heat transfer model for predicting temperature change inside food package kept in cold room. *Journal of food science and technology*, 50(2):257–265, 2013.

[49] Ricardo Badia-Melis, Ultan Mc Carthy, and Ismail Uysal. Data estimation methods for predicting temperatures of fruit in refrigerated containers. *Biosystems Engineering*, 151:261–272, 2016.

[50] Christian C Emenike, Nardus P Van Eyk, and Alwyn J Hoffman. Improving cold chain logistics through rfid temperature sensing and predictive modelling. In *2016 IEEE 19th International Conference on Intelligent Transportation Systems (ITSC)*, pages 2331–2338. IEEE, 2016.

[51] CP Tso, SCM Yu, HJ Poh, and PG Jolly. Experimental study on the heat and mass transfer characteristics in a refrigerated truck. *International Journal of Refrigeration*, 25(3):340–350, 2002.

[52] Shen Tian, Yuping Gao, Shuangquan Shao, Hongbo Xu, and Changqing Tian. Development of an unsteady analytical model for predicting infiltration flow rate through the doorway of refrigerated rooms. *Applied Thermal Engineering*, 129:179–186, 2018.

[53] Diogo L Da Silva, Christian JL Hermes, and Claudio Melo. Experimental study of frost accumulation on fan-supplied tube-fin evaporators. *Applied Thermal Engineering*, 31(6-7):1013–1020, 2011.

[54] Adrian Bejan, Jose VC Vargas, and Jong S Lim. When to defrost a refrigerator, and when to remove the scale from the heat exchanger of a power plant. *International Journal of Heat and Mass Transfer*, 37(3):523–532, 1994.